Techniques for Enhancing the Performance of Communication Systems Employing Spread-Response Precoding

by

Soosan Beheshti

Submitted to the Department of Electrical Engineering and Computer Science
in partial fulfillment of the requirements for the degree of

Master of Science in Electrical Engineering & Computer Science

at the

MASSACHUSETTS INSTITUTE OF TECHNOLOGY

February 1996

Author .....
Department of Electrical Engineering and Computer Science
January 31, 1996

Certified by .....
Gregory W. Wornell
Assistant Professor
Thesis Supervisor

Accepted by .....
Fredrick Morgenthaler
Chairman, Departmental Committee on Graduate Students

Techniques for Enhancing the Performance of Communication Systems Employing Spread-Response Precoding

by

Soosan Beheshti

Submitted to the Department of Electrical Engineering and Computer Science
on February 1, 1996, in partial fulfillment of the
requirements for the degree of
Master of Science in Electrical Engineering & Computer Science

Abstract

In wireless communication systems, various coding schemes are used to improve transmission reliability over a fading channel. A spread-response precoder, even in the absence of a coder, not only is effective in correcting errors, but also effectively transforms a Rayleigh fading channel into a simpler quasi-Gaussian one.

This research explores combining trellis coded modulation (TCM) with a spread-response precoding for transmission over a Rayleigh channel, and assesses the improvement yielded by the precoder, in terms of system complexity, delay characteristics, and probability of error performance. We will also explore a multistage postcoder for use with spread-response precoding, and assess the corresponding improved performance.

Thesis Supervisor: Gregory W. Wornell
Title: Assistant Professor

Acknowledgments

I am very grateful to my thesis supervisor, Professor Greg Wornell, for his guidance and suggestions. He provided me with the support to continue, and helped me find a sense of direction as a beginning researcher. I would like to thank him for the time and effort he has spent contributing to my work.

I also would like to thank my academic advisor, Professor Al Drake, who helped and supported me constantly during these past two years. My gratitude also extends to Professor Frank Perkins, former dean of the graduate school, for assisting me with some administrative matters near the beginning of my studies at MIT.

I wish to thank all my family and friends whom I love with all my heart.

Contents

List of Figures

List of Tables

Chapter 1

Introduction

Mobile radio communication links fall in the general category of fading channels. Just as geographically fixed transmitter/receiver radio systems suffer from degradations which are transmission medium related, *e.g.,* ionospherics in short wave radio transmission, so are mobile radio transmissions prone to such fading effects. Since the general application involves urban areas, there are many obstacles to mobile radio transmission, *e.g.,* buildings, which cause multiple reflections. This coupled with the relative motion between the transmitter and the receiver, create a multipath time-varying channel. The second important component of mobile radio communication channels is additive white Gaussian noise (AWGN) which represents both co-channel interfrence and receiver noise.

Using diversity techniques is a common method of combatting the fading problem in mobile radio communication channels [1]. Furthermore, coding methods can be employed to address not only the fading effects, but also problems raised by the AWGN. In this research we consider spread-response precoding, a diversity technique developed by Wornell [2], and employ methods to improve bit error rate.

1.1 Outline of the Thesis

In Chapter 2 we outline prerequisite background material such as the channel model and the spread-response precoder, which is a method of diversity used in both fre-

quency selective and nonselective fading channels. We also will briefly review the structure of linear, periodic, time-varying (LPTV) filters, which are used to implement practical precoders.

In Chapter 3 we first review the fundamentals of trellis coding, which is a scheme used not only in additive white Gaussian noise channels but also in fading channels. We then combine the two methods, *i.e.,* precoding and coding, and examine the resulting probability of error performances in the simulated channels. We will examine and explain the advantages and disadvantages of using this combination.

In Chapter 4 we will show how performance can be improved by developing a nonlinear receiver for the spread-response precoding scheme that more effectively combats the channel fading effects. This multistage postcoder receiver was recently introduced by Wittneben [10]. We will develop a theoretical basis for this scheme and analyze its performance.

In this research we emphasize the frequency-nonselective fading channel, but will also briefly discuss a theoretical solution for the general frequency-selective problem.

Finally, Chapter 5 contains some general conclusions, and suggests possible directions for future work.

Chapter 2

Background

2.1 System Model

In general, a mobile communication link is modeled as a time-varing, multipath, fading channel. If each multipath component is independent, zero-mean and Gaussian, the probability density function (PDF) of the envelope has a Rayleigh distribution; hence the name, Rayleigh fading channel, is used to describe such a link. If, in addition to all the changing scatterers, there are some fixed scatterers which can not be modeled as zero-mean random processes, the channel is referred to as a Ricean channel [1].

In this research, we will focus on a stationary Rayleigh fading channel. Figure 2-1 depicts the discrete-time model of such a system.

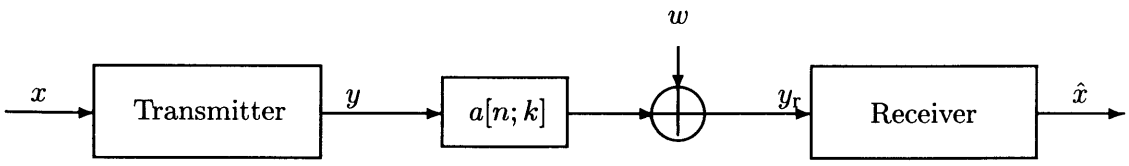

Figure 2-1: Rayleigh fading channel

As shown in the figure, the channel comprises two main components which relate the input and output according to the following equation:

$$y_r[n] = \sum_k a[n;k]y[n-k] + w[n] \quad , \tag{2.1}$$

where the fading coefficient, $a[n;k]$, represents the response of the channel at time n due to an impulse (unit sample) at time $n-k$, and $w[n]$ denotes an independent, additive, zero-mean, complex, stationary, white Gaussian noise sequence. Furthermore, $w[n]$ has variance

$$E(|w[n]|^2) = N_o W = N \ , \tag{2.2}$$

where W is the bandwidth of the baseband channel model, and N_o is the variance of the white noise before filtering at the receiver. For a fixed value of k, $a[n;k]$ can be modeled as a zero-mean complex Gaussian sequence. We assume that $w[n]$ and $a[n,k]$ are statistically independent of the input to the channel. Since in most mobile communication channels the channel coefficient due to path delay k_1 is uncorrelated with that associated with path delay k_2, we may write the following uncorrelated scattering equation

$$E([a[n;k_1], a[n+l;k_2]) = R_a[l, k_1 - k_2]\, \delta[k_1 - k_2] \ , \tag{2.3}$$

where $R_a[l, \Delta k]$ is an autocorrelation function that gives the average output power as a function of the time delay, l, and the difference in observation times, Δk. In particular, $R_a[l,0] = R_a[l]$ is called the *multipath intensity profile* or *delay power spectrum*, since it denotes the average power output of the channel as a function of the time delay [1]. We may also define the time-variant channel frequency response as follows[1]

$$A(\omega;n] = \sum_k a[n;k] e^{j\omega k} \ . \tag{2.4}$$

This frequency response, which is stationary in both n and ω, has the following mean and variance:

$$E(A(\omega;n]) = 0 \tag{2.5}$$

$$E(|A(\omega;n]|^2) = \sigma_a^2 \ . \tag{2.6}$$

[1]We use $(\cdot)$ to denote continuous-valued arguments and $[\cdot]$ to denote discrete-valued arguments. Therefore, for functions of two arguments where the first is continuous and the second is discrete, we use the hybrid notation $[\cdot,\cdot)$.

In following sections we assume that the original M-PSK sequence to be sent has energy E_s, and the additive noise has variance N.

2.1.1 Additive White Gaussian Noise (AWGN) Channels

If we ignore the fading component, as in Figure 2-2, we are left with one of the simplest types of channels, additive white Gaussian noise (AWGN) channel. For a multipath fading channel with an additive Gaussian noise, by using an AWGN model, we can define an *optimum* probability of error performance, achievable for the channel considered. The Gaussian channel is important for providing a lower bound on error (*i.e.*, an upper bound on quality) and, hence, a bound for system performance.

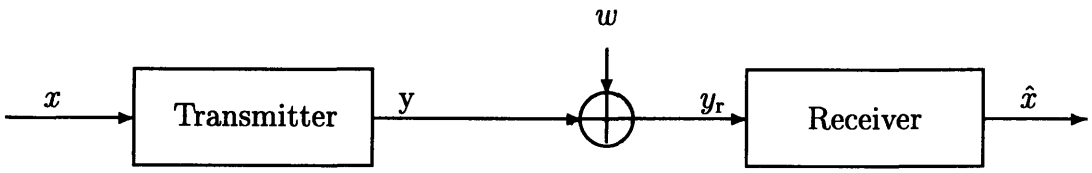

Figure 2-2: AWGN channel

In general, the probability of error for the AWGN channel is given by [1]

$$\Pr(\varepsilon) = Q\left(d_{\min}\sqrt{\frac{1}{2\xi}}\right) \quad , \tag{2.7}$$

where

$$Q(v) = \frac{1}{\sqrt{2\pi}}\int_v^\infty e^{-t^2/2}dt, \tag{2.8}$$

and $d_{\min}$ is the minimum Euclidean distance between normalized symbols sent by the transmitter, and ξ represents the inverse of the sequence SNR

$$\xi = \frac{N}{E_s} \quad . \tag{2.9}$$

For example, in the case of 4-PSK, d_{min} is $\sqrt{2}$ and the probability of error is

$$\Pr(\varepsilon) = Q\left(\frac{1}{\sqrt{\xi}}\right) \quad . \tag{2.10}$$

2.2 Spread-Response Precoders

Figure 2-3 shows a precoder and postcoder system used in a fading channel. The input sequence $x[n]$, is the original sequence to be transmitted, or a modulated sequence with a smaller symbols/sec rate, *i.e.,* an M-PSK sequence.

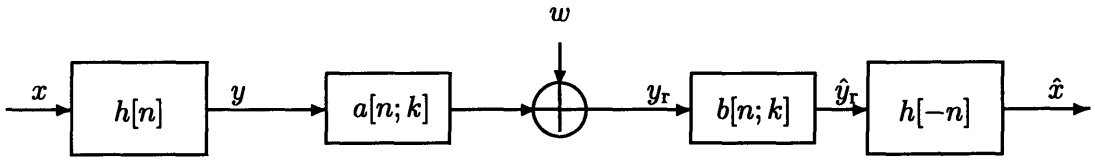

Figure 2-3: Channel with precoder

The basic idea behind the precoder is to overcome the fading effect through extraction of the average channel characteristics. Wornell [2] has developed an effective method which involves spreading the transmission of each symbol over a large number of time samples. This spreading can be achieved through the use of a linear time-invariant (LTI) filter $h[n]$, as a precoder. Therefore, the transmitted sequence is

$$y[n] = \sum_k x[n] * h[n-k] \ . \tag{2.11}$$

In order to measure the dispersion of a unit-energy precoder, we use the dispersion factor $\mathcal{D}_h$, which is given by [2]

$$\mathcal{D}_h \ = \ \frac{1}{\sum_n h^4[n]} \ . \tag{2.12}$$

Good spreading characteristics are achievable by maximizing the dispersion factor. Furthermore, it is highly desirable for the precoder to be a *lossless* (all-pass) filter and it should satisfy

$$h[n] * h[-n] \ = \ \delta[n] \ . \tag{2.13}$$

As a result of this property, we have

$$\sum_n h^2[n] = 1 , \tag{2.14}$$

$$h^{-1}[n] = h[-n] . \tag{2.15}$$

However, this condition is not exactly achievable. In order to approach this criterion we may define the losslessness factor $\mathcal{L}_h$ as follows [2]

$$\mathcal{L}_h = \frac{1}{\sum_n (\Phi_h[n] - \delta[n])^2} , \tag{2.16}$$

where $\Phi_h[n] = h[n] * h[-n]$, and large $\mathcal{L}_h$ corresponds to a filter that is nearly lossless.

Letting kernel $b[n;k]$ denote the time-varying equalizer response, the output of the equalizer can be written as (*cf.* Figure 2-3)

$$\hat{y}_r[n] = \sum_k b[n;k] y_r[n-k] + \sum_k b[n;k] w[n-k] . \tag{2.17}$$

Using $h[n]$ as the precoder at the transmitter and $h[-n]$ as the postcoder at the receiver, Wornell [2] has shown that the system depicted by Figure 2-3 asymptotically behaves like an additive Gaussian channel. Consequently, an uncorrelated symbol sequence $x[n]$ will yield a postcoder output $\hat{x}[n]$ which converges, in the mean-square sense, for each n, as in the following

$$\tilde{x}[n] \xrightarrow{\text{m.s.}} \mu_c x[n] + v[n] , \tag{2.18}$$

where $v[n]$ is a complex-valued, zero-mean, white, marginally Gaussian noise sequence, uncorrelated with the input sequence $x[n]$, and with variance

$$\text{var } v[n] = E_s \sigma_c^2 + N(\sigma_b^2 + |\mu_b|^2) . \tag{2.19}$$

In (2.19), E_s denotes the energy of the symbol sequence $x[n]$, while μ_b and σ_b^2 denote the mean and variance, respectively, of kernel $B(\omega;n]$. Furthermore, μ_c in Ex-

pression (2.18) and σ_c^2 in (2.19) are the mean and variance, respectively, of $C(\omega, n]$, the frequency response of the composite linear system; the system is formed by cascading the channel corresponding to kernel $a[n;k]$, with the equalizer corresponding to $b[n;k]$, *i.e.*,

$$c[n;k] = \sum_l b[n;l]a[n-l;k-l] \ . \tag{2.20}$$

The fact that, for sufficiently long $h[n]$, the Rayleigh fading channel behaves asymptotically like an AWGN channel, allows computation of the probability of error for a 4-PSK sequence, using (2.10)

$$\Pr(\varepsilon) = Q(\sqrt{\gamma}) \ , \tag{2.21}$$

where γ is the equivalent SNR, which in this case is

$$\gamma = \frac{|\mu_c E_s|^2}{E_s\sigma_c^2 + N(\sigma_b^2 + |\mu_b|^2)} \ . \tag{2.22}$$

2.2.1 Frequency-Nonselective Fading Channel

Whenever

$$a[n;k] = a[n]\delta[k] \ , \tag{2.23}$$

the channel output may be expressed as

$$y_r[n] = a[n]y[n] + w[n] \ , \tag{2.24}$$

and we are restricted to the frequency-nonselective model. In this case, the equalizer is also of the form

$$b[n;k] = b[n]\delta[k] \ . \tag{2.25}$$

In order to maximize the equalizer output SNR, *i.e.*, γ in (2.22), Wornell [2] has shown that $b[n]$ is of the form:

$$b[n] \propto \frac{a^*[n]}{|a[n]|^2 + \xi} \ , \tag{2.26}$$

where ξ is defined in (2.9). With this equalizer the SNR at the output of the postcoder is now given by [2]

$$\gamma = E\left[\frac{|a|^2}{|a|^2+\xi}\right] \ , \tag{2.27}$$

which can be written as follows

$$\gamma = \frac{1}{\xi e^{\xi} E_1(\xi)} - 1 \ , \tag{2.28}$$

where $E_1(\cdot)$ denotes the exponential integral

$$E_1(v) = \int_v^{\infty} \frac{e^{-t}}{t} dt \ . \tag{2.29}$$

Note that all these results are valid only for sufficiently long $h[n]$, which corresponds to the scenario where the system is well approximated by the equivalent AWGN channel model.

2.2.2 Frequency-Selective Fading Channel

For cases where the transmission bandwidth is larger, we consider the more general frequency-selective fading channel. Recall that in the frequency-nonselective channel, the *coherence bandwidth* of the channel $(\Delta f)_c$ is much larger than the bandwidth W of the signal, and we have $W \ll (\Delta f)_c$. For the frequency-selective case, on the other hand, the coherence bandwidth is far exceeded by W, and we have $W \gg (\Delta f)_c$ [1].

Furthermore, we have assumed that the channel is *slowly* fading for which the *Doppler spread* B_d is much smaller than the coherence bandwidth; namely, $(\Delta f)_c \gg B_d$ [1].

With this assumption we have the slowly time-varying channel frequency response $A(\omega; n]$. Therefore, the equalizer $B(\omega; n]$ will also be slowly time-varying, and we have:

$$C(\omega; n] \approx A(\omega; n] B(\omega; n] \ . \tag{2.30}$$

Furthermore,

$$\sigma_c^2 = \text{var}\,[C(\omega;n]] \tag{2.31}$$

$$\sigma_b^2 + |\mu_b|^2 = E[|B(\omega;n]|^2] \tag{2.32}$$

Therefore, using the definition of γ in (2.27), we have

$$\gamma = \frac{|E(AB)|^2}{\text{var}\,[AB] + \xi E(|B|^2)}, \tag{2.33}$$

where ξ is defined in (2.9). Due to wide sense stationarity, γ is independent of both n and ω. Also, it can be seen that γ is identical in form to that in (2.28). Using a method analogous to that which was used for the frequency-nonselective channel for finding the optimal equalizer [2], we have

$$B(\omega;n] \propto \frac{A^*(\omega;n]}{|A(\omega;n]|^2 + \xi}\,. \tag{2.34}$$

2.3 Linear Periodic Time-Varying (LPTV) Precoders

Alternatively, an LPTV system may be used as the LTI precoder, as shown in Figure 2-4. This orthogonal system provides the optimum linear diversity with very low computational complexity compared to the general precoder defined in Section 2.2.

The equation governing the input/output relationship of the LPTV precoder with period-K is given by

$$y[n] = \sum_{l=-\infty}^{+\infty} \sum_{m=0}^{K-1} x[lK - m]h_k[n - lK], \tag{2.35}$$

where

$$\mathbf{H}[n] = \begin{bmatrix} h_0[n] & h_1[n] & \cdots & h_{K-1}[n] \end{bmatrix}^T. \tag{2.36}$$

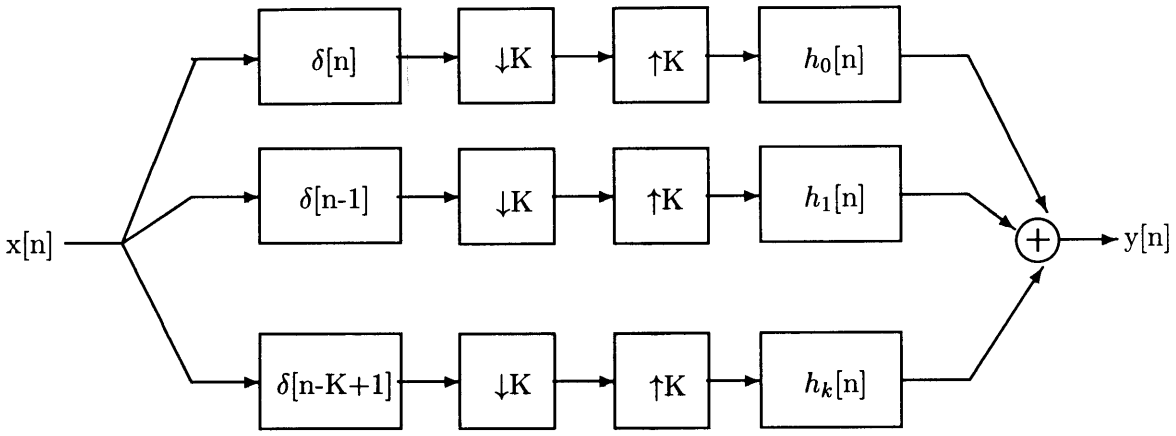

Figure 2-4: Linear periodically time-varying precoder

The Fourier transform of $\mathbf{H}[n]$ is given by

$$\mathcal{H}(\omega) = \sum_n \mathbf{H}[n]e^{-j\omega n}d\omega = \begin{bmatrix} H_0(\omega) & H_1(\omega) & \cdots & H_{K-1}(\omega) \end{bmatrix}^T, \tag{2.37}$$

which in polyphase form is

$$\mathcal{H}(j\omega) = \mathcal{Q}(K\omega)\Delta(\omega), \tag{2.38}$$

where $\Delta(\omega)$ is the delay chain of order K,

$$\Delta[n] = \begin{bmatrix} 1 & e^{-j\omega} & \cdots & e^{-j\omega(K-1)} \end{bmatrix}^T. \tag{2.39}$$

The polyphase matrix $\mathcal{Q}(\omega)$ has the property

$$\mathcal{Q}(\omega)\mathcal{Q}'(\omega) = I, \tag{2.40}$$

where $\mathcal{Q}'(\omega)$ is the conjugate-transpose of $\mathcal{Q}(\omega)$. The postcoder is the transpose of the precoder shown in Figure 2-4. Wornell [3] has discussed using related systems in multiuser channels.

When we use LPTV system as a precoder, there is no advantage to using $K > 2$. The important parameter is the $h_i[n]$ filter length, which effectively is the length of the precoder in this system.

Furthermore, when the length of the filter, L, is a power of 2, $h_i[n]$ takes on as values only $\pm\frac{1}{\sqrt{L}}$. It is worth mentioning that fixed-length filters with

$$\mathcal{D}_h = L \tag{2.41}$$

$$\mathcal{L}_h = \infty \ . \tag{2.42}$$

maximize the dispersion factor $\mathcal{D}_h$ and the losslessness factor $\mathcal{L}_h$, defined in Section 2.2, among all possible precoders. In this research we use such LPTV systems as precoders. Table 2.1 shows an example of an LPTV precoder with $K = 2$ and $L = 8$.

$n=$	0	1	2	3	4	5	6	7
$\sqrt{8}h_0[n]$	+1	+1	+1	−1	+1	+1	−1	+1
$\sqrt{8}h_1[n]$	+1	+1	+1	−1	−1	−1	+1	−1

Table 2.1: LPTV precoder with length eight and period two.

2.3.1 Performance on Frequency-Nonselective Channel

Figure 2-5 shows the results corresponding to LPTV filters of varying lengths used as precoders in a frequency-nonselective channel. As the figure indicates, by increasing the precoder length the performance approaches the theoretical result shown in Section 2.2.

Although the performance has improved without requiring any additional power or bandwidth, as the results show there is still a considerable difference between the system performance with the precoder in a fading channel, and that of the AWGN channel. We will discuss methods for further performance improvement in the sequel.

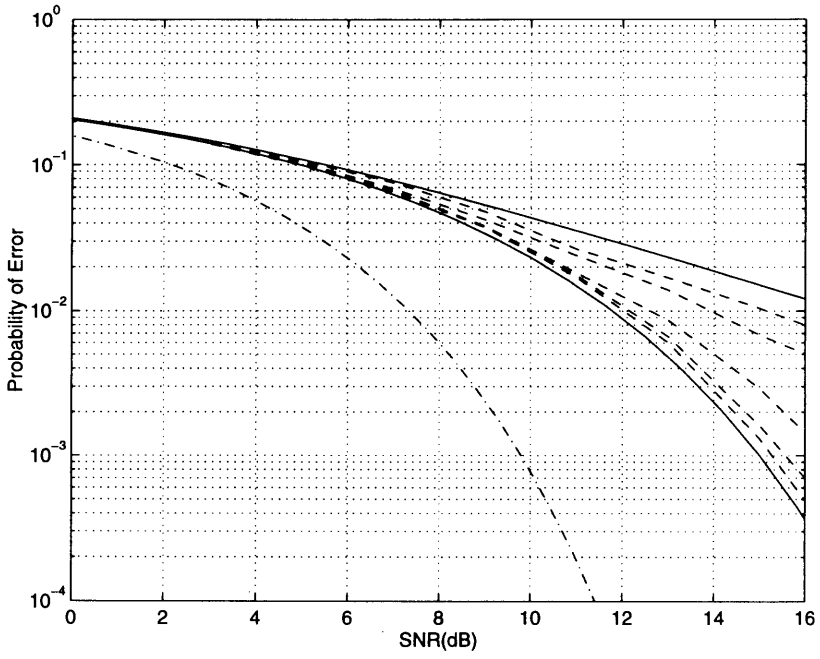

Figure 2-5: *Probability of error for 4-PSK sequence on the Rayleigh fading channel: The successively lower solid curves represent the performance without any precoder and the performance for infinite-length precoder. The successively lower dashed curves correspond to the performance of precoders with lengths: L=2,4,16,64, and 256, respectively. The dash-dotted curve represents the performance of the AWGN channel using an uncoded 4-PSK sequence.*

Chapter 3

Trellis Coding and Spread-Response Precoder in Fading Channels

3.1 Introduction

We showed in Chapter 2 that through precoding we can overcome the effects of channel fading. In this chapter we would like to combine the precoder with some coding methods in order to improve the probability of error performance. The coder we introduce uses trellis coded modulation (TCM), which is a popular coding scheme in systems with or without fading [1].

The coding structure of TCM is the same as that in convolutional coding, with modulation added as part of the coding scheme. By passing the information sequence through a finite, binary filter, useful redundancy is added to the sequence which makes the independent channel-error correctable in the receiver. Also, through modulation we can control the bandwidth of the transmitted sequence, while simultaneously coding it. If there are n output bits for each k-bit input sequence, the coder is called a TCM with rate k/n.

A binary input along with a finite number of shift registers in the coder makes a

Markov chain model. Based on the structure, some of the registers of the TCM coder represent the states of the Markov chain.

A rate-2/3 TCM, shown in Figure 3-1(a), is an example of such a coder. As the figure indicates, 3 output bits of the convolutional coders are mapped to 8-PSK symbols (*cf.* Figure 3-1(b)). For this coder, bits registered on forward delays T_2 and T_3 determine the states of the Markov chain. Figure 3-1(c) shows one segment of the trellis diagram of this structure for the 4-state coder, where each node represents one possible state, and the numbers on the links connecting two nodes denote the output which yields the corresponding change of state. Furthermore, for each link we have a specific input, enclosed in parentheses on the link.

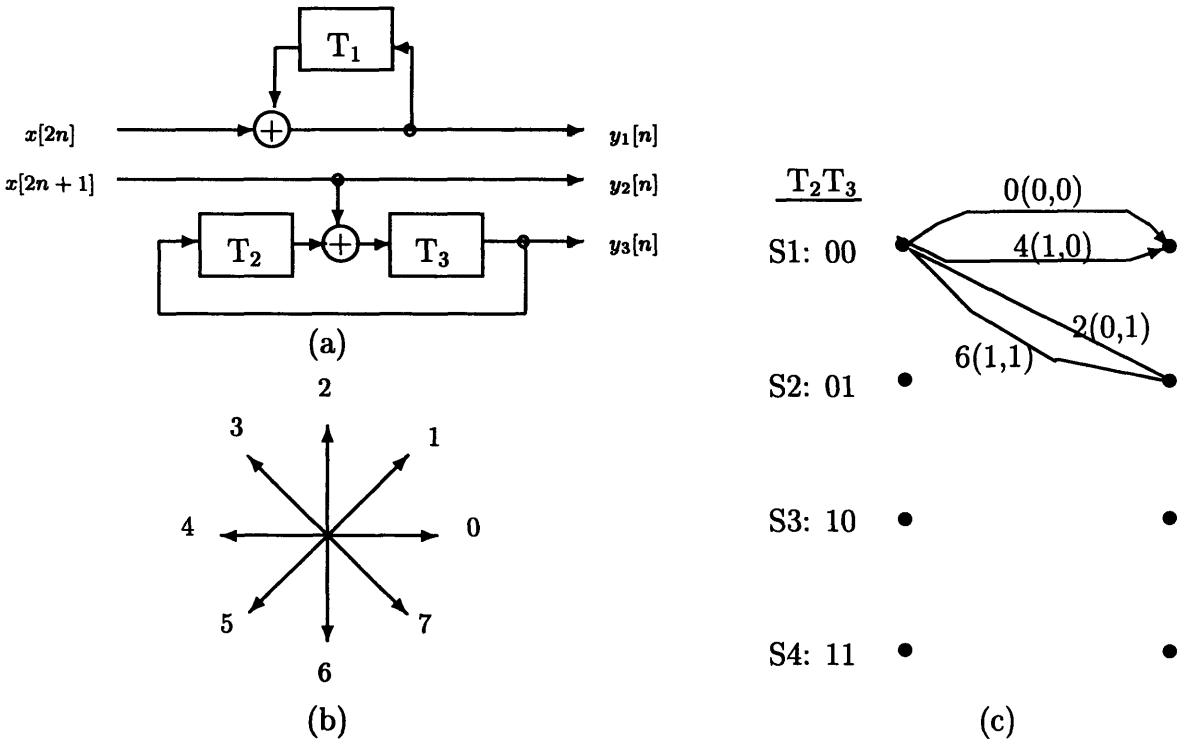

Figure 3-1: (a) Trellis1, (b) 8-PSK symbol representation for the output of Trellis1 (c) State-space representation of Trellis1.

Decoding at the receiver is performed using ML detection. Namely, the optimum decoding scheme is to search for the path which most likely resulted in the received sequence. Normally, due to noise, the receiver may not identify the correct path in trellis diagram, meaning that the chosen path diverges from the correct one at some time n, and remerges at a later time $n + l$. When this happens we say that an error

event of length l has taken place. The free distance of a TCM, d_{min}, is the minimum Euclidean distance between a pair of paths forming the *error event path* corresponding to the smallest l. Considering the trellis diagram of Trellis1 (*cf.* Figure 3-1(c)), the minimum Euclidean distance for the all-zero path is the distance between symbol 4 and symbol 0 shown in Figure 3-1(b), which is

$$d_{\min} = |j - 1| = 2. \tag{3.1}$$

Among various decoding techniques for TCM, the Viterbi algorithm is the most widely used. In the receiver decoding block, if the signal is processed prior to making the decision as to which transmitted symbol it corresponds to, the designation is called a "soft decision." Alternatively, if a partial decision is made about the received signal prior to the application of the Viterbi algorithm *e.g.*, quantizing the received signal, it is called a "hard decision." In our application we use the soft-decision Viterbi algorithm to decode the TCM coded sequences. Also of significance is the decision depth, which is the number of symbols used in the algorithm to decode a single symbol at the receiver. Usually a decision depth of about 3 times the number of states is sufficient to make a decision at each decoding stage [4].

In order to analyze the theoretical aspects of a fading channel with precoder and coder, we outline the performance of the AWGN channel using trellis coding in the following section.

3.2 Trellis Coding in AWGN channel

Consider an AWGN channel with a trellis coder and a Viterbi decoder (*cf.* Figure 3-2).

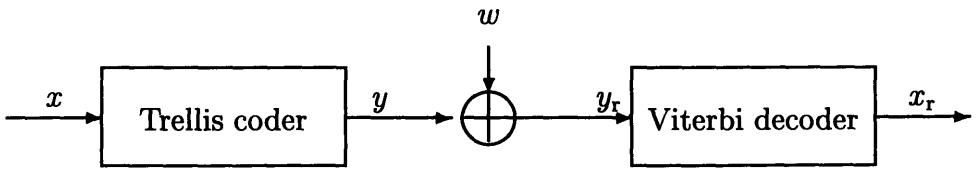

Figure 3-2: AWGN Channel with trellis coder

In this section we shall find the probability of error for such a channel. We can represent the probability of error as

$$\Pr(\varepsilon) = \sum_i \text{pr}(i, \varepsilon) = \sum_i \text{pr}(\varepsilon|i) \cdot \text{pr}(i), \tag{3.2}$$

where $\text{pr}(\varepsilon|i)$ is the conditional probability of error, given the sequence corresponding to path i has been sent, and $\text{pr}(i)$ is the apriori probability of transmission of the sequence path i. In most cases the structure of the TCM is such that the $\text{pr}(\varepsilon|i)$ is the same for all i. Therefore, we consider the case of an all-zero path ($i = 1$) to find the error. Using the union bound, we have

$$\Pr(\varepsilon) = \text{pr}(\varepsilon|1) \leq \sum_{j \neq 1} \text{pr}(j|i = 1) \, , \tag{3.3}$$

where $\text{pr}(j|i)$ is the conditional probability of detecting path j given that path i is the correct path. In the case of additive white Gaussian noise, the terms in the right-hand side are $Q(\cdot)$ functions. Hence, the bound can be written as

$$\Pr(\varepsilon) \leq D(d_{min}) Q\left(d_{\min}\sqrt{\frac{\alpha}{2}}\right) + \Phi(\alpha) \quad , \tag{3.4}$$

where

$$\alpha = \frac{E_s}{N} \, , \tag{3.5}$$

N is the noise variance $w[n]$, and E_s is the energy of the received sequence, $y_r[n]$. Furthermore, $D(d_{\min})$ is a constant which depends on the distance structure of the trellis codes, and denotes the number of paths with a Euclidean distance of d_{min} from the all-zero path. Moreover, $\Phi(\cdot)$ is a positive function of α, and is the sum of $Q(\cdot)$ functions, defined in (2.8), corresponding to Euclidean distances which are larger than $d_{\min}$, and for which

$$\lim_{\alpha \to \infty} \Phi(\alpha) = 0.$$

Note that if $D(d_{\min})$ is not a large number, which is the case with almost all TCM schemes, it is possible to ignore this coefficient for high SNRs. Consequently, at high

SNRs, *i.e.*, large α, we have

$$\Pr(\varepsilon) \approx Q\left(d_{\min}\sqrt{\frac{\alpha}{2}}\right). \tag{3.6}$$

Moreover, in order to calculate the probability of error per bit, this calculated probability of error would be multiplied by the average bit-error occurred when the wrong path corresponding to the minimum Euclidean distance, $d_{\min}$, is selected.

As the expression for the probability of error shows, the performance of TCM can be improved by enlarging $d_{\min}$. In order to obtain larger minimum Euclidean distance the number of states must grow. However, the number of states has an exponential relation with the time delay of the Viterbi decoder; therefore, there should be a trade-off between time delay and performance improvement, in designing and implementing the TCM coder.

3.2.1 Performances in AWGN Channel using TCM

In this section we use three TCM coders, with rate 2/3, introduced by Ungerboeck [5, 6], as follows:

1. A 4-state trellis coder, as shown in Figure 3-1.
2. An 8-state feedback-free trellis code, as shown in Figure 3-3.
3. An 8-state trellis coder with feedback, as shown in Figure 3-4.

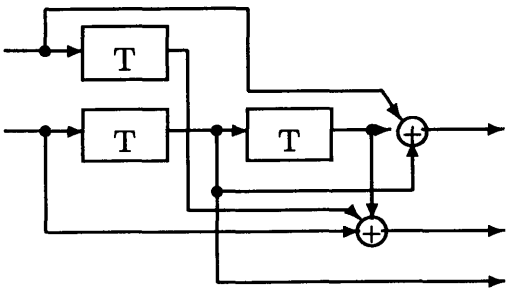

Figure 3-3: Trellis2

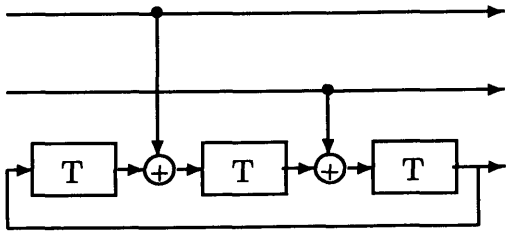

Figure 3-4: Trellis3

The minimum Euclidean distances of Trellis2 and Trellis3, *i.e.*, $d_{\min 2}$ and $d_{\min 3}$, are given by [1]

$$d_{\min 2} = \sqrt{(\sqrt{2})^2 + 2^2} = \sqrt{6} \qquad d_{\min 3} = \sqrt{(\sqrt{2})^2 + 2^2} = \sqrt{6}\,. \tag{3.7}$$

In our experiments the Viterbi algorithm with a decision depth of 30 is used. The performance of three Trellis codes in AWGN channel with binary input symbols is depicted in Figure 3-5.

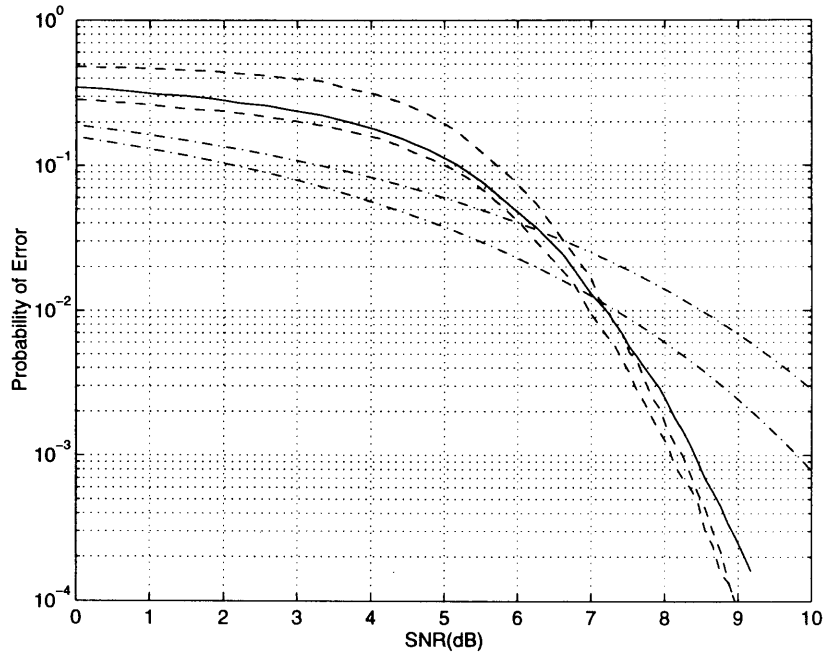

Figure 3-5: *Probability of error in an AWGN channel using TCM: The solid curve is the performance usig Trellis1. The successively lower dashed curves denote the performance using Trellis3 and Trellis2, respectively. The successively lower dash-dotted curves are the performances of uncoded 8-PSK and 4-PSK sequences on the channel.*

As the results in the figure indicate, for low SNRs the probability of error corresponding to the channel with Trellis coding is worse than that of a channel without coding (4-PSK or even 8-PSK performances). These performances show that at low SNRs minimizing the probability of error symbol-by-symbol in an uncoded transmission, is more efficient than the Viterbi algorithm in a coded transmission, which at each step minimizes the probability of error of the symbol strings, based on a certain

decision depth.

3.2.2 TCM in Fading Channel

In this section we consider the frequency-nonselective fading channel in the presence of trellis coding. Figure 3-6 shows the channel and the equalizer.

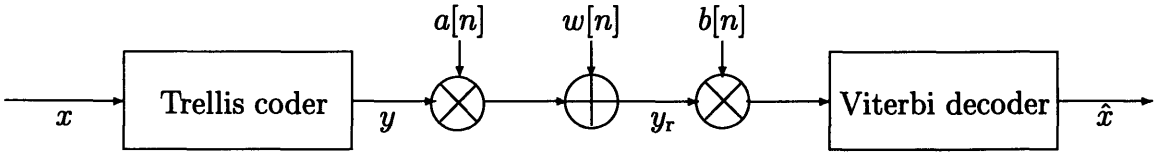

Figure 3-6: Trellis coder in fading channel

The optimum equalizer $b[n]$ is the same as that which we use in the fading channel without any coding, *i.e.*,

$$b[n] = a^*[n] \; . \tag{3.8}$$

For the fading channel the design of the code for optimum performance is not guided by just the length of the shortest *error event path.* Rather, there are additional properties affecting the performance of the TCM. Divsalar [7] has shown that the probability of error is upper bounded by

$$\Pr(\varepsilon) \leq \frac{K}{\alpha^{L_T}} \; , \tag{3.9}$$

where α is the SNR of the transmitted sequence, defined in (3.5). L_T is the number of nonzero pairwise distances between the symbols along the branches of the shortest error event path and those along the correct path; and K is a constant which depends on the distance structure of the TCM. For example, consider a trellis code with the shortest event path for the all-zero path shown in Figure 3-7. The figure depicts a 4-PSK transmitted signal (output of the TCM coder), with the numbers on each branch corresponding to the transmitted signal. As is shown, the all-zero path sequence comprises branches with 1, which represents the 00 code. Since there are two symbols in the shortest event path which are different than those of the all-zero path, L_T is 2.

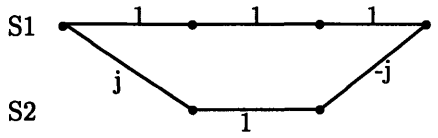

Figure 3-7: Shortest event path for the all-zero path.

It can be shown that the upper bound of the probability of error corresponding to Trellis1 in an AWGN channel is [1]

$$\Pr(\varepsilon) = \frac{1}{2}\left(1 - \frac{1}{\sqrt{1+2/\alpha}}\right) . \tag{3.10}$$

where α is as defined in (3.5). We note that for high SNRs, $\Pr(\varepsilon) \approx 1/2\alpha$ which is consistent with Divsalar's approximations. Figure 3-8 shows the convergence of the performance to this theoretical bound.

3.2.3 Performance in Fading Channel using TCM

We have simulated a frequency-nonselective fading channel in the presence of Trellis1, Trellis2, and Trellis3. The results of the performances are shown in Figure 3-8. As the figure indicates, we still have the same behavior at low SNRs that we had in the AWGN channel with trellis coding.

3.3 Combination of TCM and Spread-Response Precoder

In this section, we show simulation results corresponding to the combination of both TCM and precoder, as in Figure 3-9.

As the results of Section 2.2 indicate, for sufficiently long precoders the subsystem inside the dashed box can be assumed to asymptotically approach an AWGN channel. Therefore, for this new channel model the approximation of the probability of error

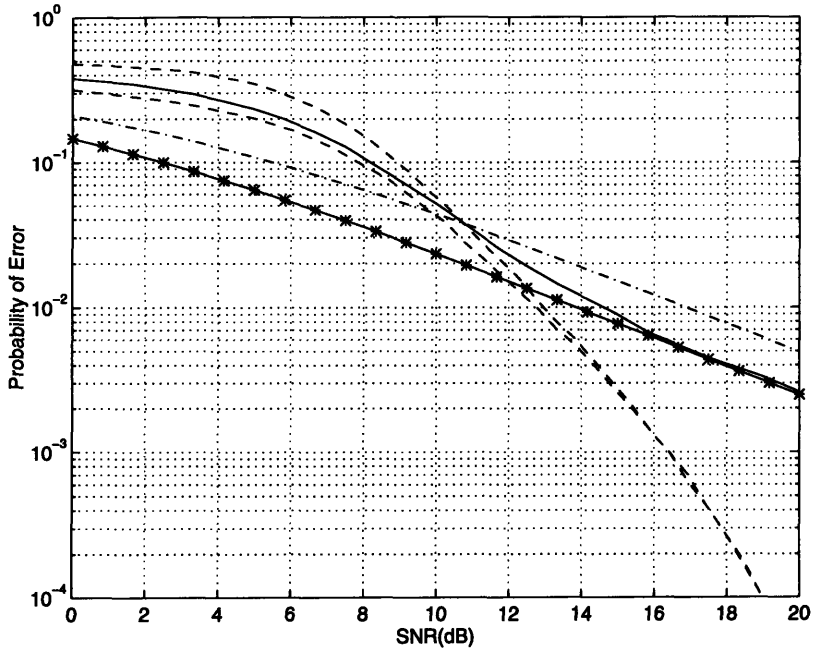

Figure 3-8: *Probability of error in a fading channel using TCM: The solid curve is the performance using Trellis1. The solid line with star is the theoretical approximation of the probability of error using Trellis1,* (3.10)*. The successively lower dashed curves correspond to the performances using Trellis3 and Trellis2, respectively, and the dash-dotted curve is the performance of uncoded 4-PSK sequence.*

in high SNRs would be (*cf.* (3.6))

$$\Pr(\varepsilon) \approx Q\left(d_{\min}\sqrt{\frac{\gamma}{2}}\right), \tag{3.11}$$

where γ is the SNR at the input of the Viterbi decoder, defined in Equation (2.22) and $d_{\min}$ is the minimun Euclidean distance of the trellis coder. Using the same argument as that used in Section 3.2, the probability of error is upper bounded by a sum of $Q(\cdot)$ and for high SNRs the probability of error is approximately equal to the first

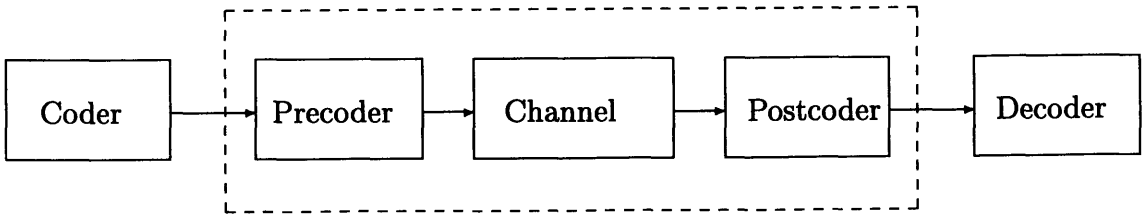

Figure 3-9: Precoding and coding system

$Q(\cdot)$ function, corresponding to $d_{\min}$.

3.3.1 Performance in Fading Channel using TCM/Precoder

Figure 3-10 shows the results of using a trellis coder and a precoder with a sufficiently long length. In Figure 3-11 we show the performance results corresponding to using Trellis2 along with precoders having different lengths.

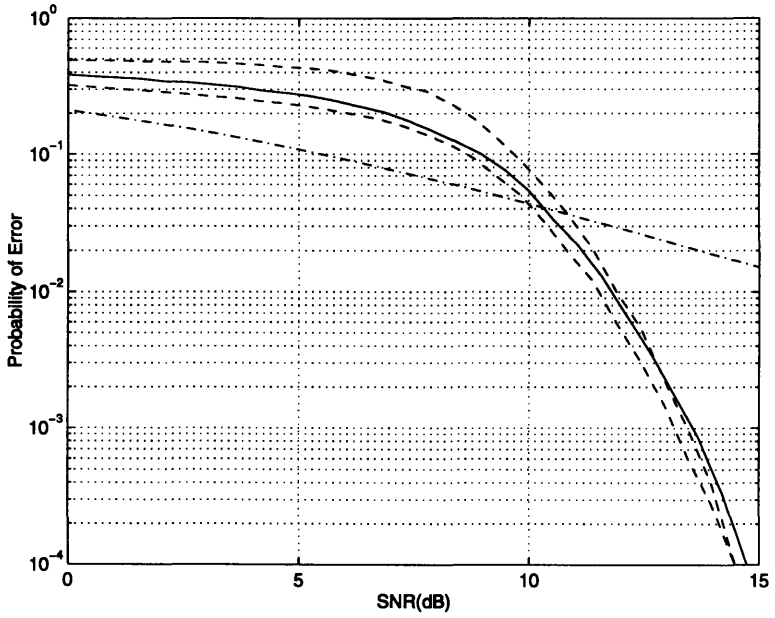

Figure 3-10: *Probability of error in a fading channel, using precoder with length 256 and TCM: The solid curve is the performance using Trellis1. The succecively lower dashed curves are the performances using Trellis3 and Trellis2 respectively. The dash-dotted curve is the performance of uncoded 4-PSK sequence with no precoding.*

3.3.2 Theoretical Probability of Error

We have seen that there is a theoretical expression for probability of error at high SNRs when we use the TCM with an AWGN channel. A similar strategy can be used with the combination of spread-response precoding and TCM in a fading channel. Figure 3-12 depicts the two cases for Trellis2.

As figure suggests the actual probability of error curve in the AWGN channel converges to the theoretical bound at a much lower SNR than that of the fading

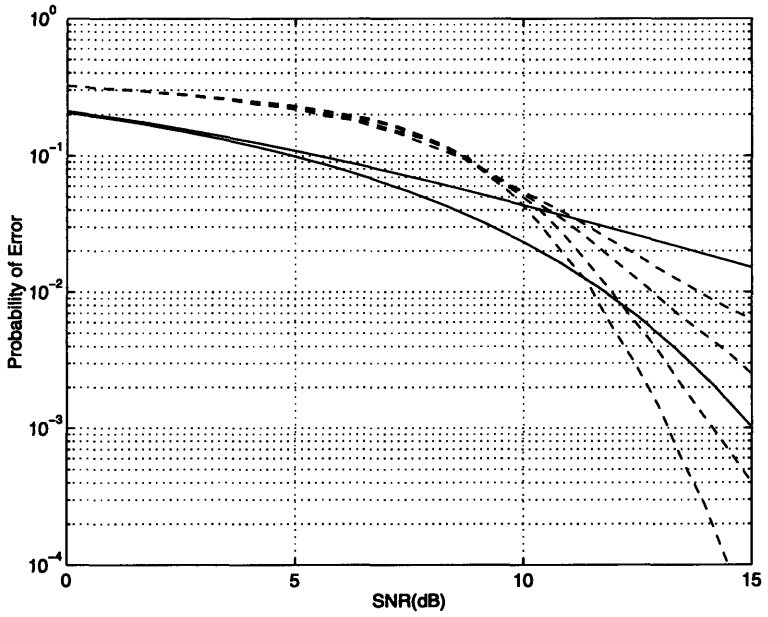

Figure 3-11: *Probability of error in a fading channel, using precoder and Trellis2: The successively lower dashed curves correspond to the performance using the precoder with lengths:4,16,64,256. The successively lower solid curves are the performances of uncoded 4-PSK sequence, without precoding and with sufficiently long precoder.*

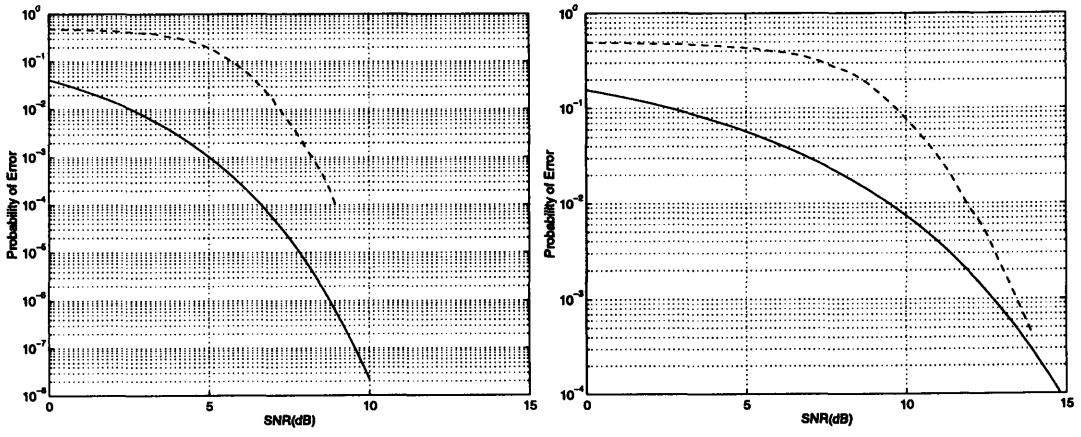

(a) (b)

Figure 3-12: *Probability of error in (a) AWGN channel, (b) fading channel, with precoder and Trellis3: dashed curve is the results of using Trellis3 coder and the solid curve is the approximated probability of error for high SNRs,* (3.6),(3.11).

channel with precoder. The reason for such behavior can be explained as follows. Figure 3-13 shows the γ in (2.22) as a function of the SNR. As the figure indicates, $\gamma(\text{SNR}) \leq \text{SNR}$ for all SNRs above 1. This behavior of $\gamma(\text{SNR})$ proves that theoretical as well as actual probabilities of error corresponding to the fading channel with coder and precoder, *cf.* Figure 3-12(b), are effectively nonlinear expanded versions of those of the TCM in an AWGN channel, *cf.* Figure 3-12(a).

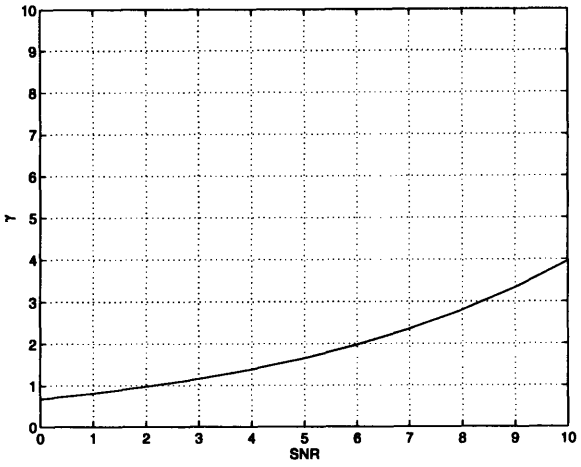

Figure 3-13: γ versus SNR.

3.4 Comparing the Performances

Figure 3-14 depicts the results of using a trellis coder with a sufficiently long precoder. As the figure shows, at low SNRs the best performance is that of the system with precoder only, and the worst performance is that of the channel with both precoder and trellis coder. It seems that the problems identified for the Gaussian channel in low SNRs, *cf.* Section 3.2, are just as relevant in this case. Also at low SNRs the performance of channel using TCM/precoder degrades a small amount relative to that of the scheme using the trellis coder alone. When using both Trellis1 and Trellis2 in the region around 12dB, the performances reverse and for the higher SNRs the performance of the system with the combination precoder/TCM is better.

In general, d_{min} of a trellis coder structure increases by increasing the number of states. Considering the exponential relation between the number of states and the

Viterbi algorithm delay, it clearly is impossible to achieve the arbitrary large $d_{\min}$ and hence high performance. However, as the results of this chapter show, considerable improvement can be obtained by using trellis codes with an acceptable number of states (4 and 8). In the following chapter, we will explore another approach to improving the spread-response precoder performance.

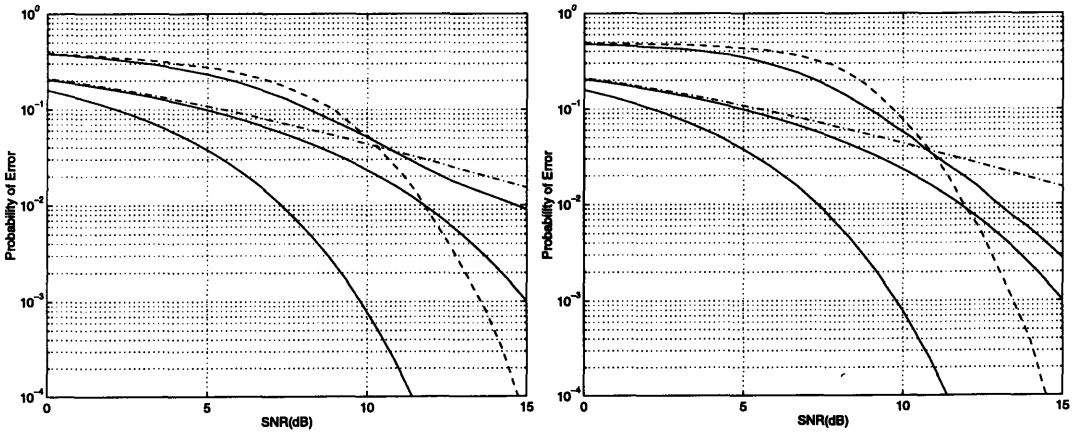

Figure 3-14: *Probability of error in fading channel, (a) depicts the performances using Trellis1 and (b) depicts the performances using Trellis3: In both figures the dash-dotted line is the performance of uncoded 4-PSK sequence without precoder. The successively lower solid curves denote the performance using TCM and the performance using precoder alone and the performance of uncoded 4-PSK sequence on AWGN channel. The dashed curve represents the performance of channel using both TCM and precoder.*

Chapter 4

Spread-Response Precoders with Improved Postcoder in Fading Channels

4.1 Introduction

In Chapter 2 we outlined the use of spread-response precoding in a mobile communication fading channel. Although with such a precoder we acquire the proper time diversity in the fading channel, the strategy also generates intersymbol interference (ISI). Wornell [2] has shown how a sufficiently long precoding filter $h[n]$, effectively transforms a fading channel into a marginally Gaussian channel. An important difference between the transmission scheme using precoding, and a traditional AWGN channel is that the noise in the former has a component which is dependent on the energy of the original signal (*cf.* (2.19)). This signal-dependent component is due to ISI. One method for recovering the transmitted signal is to use maximum likelihood (ML) decoders in the receiver. Since for a finite-length precoder, the number of distinct symbols to be sent are finite, we can in principle use the Viterbi algorithm [9] for decoding. However, the complexity of this optimal decoder grows exponentially with the length of the precoder, which in practice is prohibitive for spread-response

precoders with even moderate lengths of interest.

A multistage postcoder scheme was recently proposed by Wittneben [10] and is aimed at partially cancelling the ISI effect. In this chapter we analyze and explore further developments of this suboptimal decoding scheme.

In what follows, we continue to assume that the receiver has perfect side information on the fading parameter, $a[n;k]$. Furthermore, we will show that using LPTV systems in lieu of the FIR precoder $h[n]$, significantly reduces the computational complexity of postcoding.

4.2 Frequency-Nonselective Fading Channel

We begin the discussion with a simple model as described in Section 2.2.1. Furthermore, we assume for convenience that the channel is memoryless, and $a[n]$ is a statistically independent fading coefficient sequence. The first stage of the postcoder is the same as that which was described in Chapter 2. We shall explore this stage of the postcoder in greater detail in order to gain valuable insight in our effort to design and construct the remaining subsystems of the decoder.

4.2.1 First Stage of the Postcoder

Figure 4-1 shows the channel model along with the first stage of the decoding structure. Although we know the characteristics of the system's second-order statistics (*cf.* Section 2.2), let us further examine the processing effects.

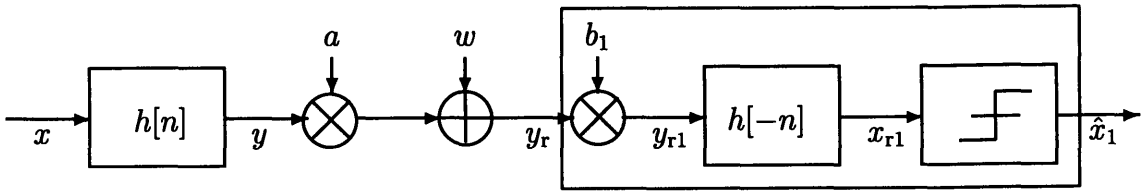

Figure 4-1: Channel and first stage of the postcoder

The input $x[n]$ is a sequence of zero-mean, statistically independent binary symbols. Another assumption which does not affect the general procedure is that the

average energy-per-symbol is unity, *i.e.*, $E[|x[n]|^2] = E_s = 1$ ($x[n] = \pm 1$). Furthermore, $a[n]$ is a complex white Gaussian sequence with $\text{var}(a[n]) = 1$, and $w[n]$ is an additive Gaussian random sequence with variance N, also the precoder is FIR filter $h[n]$ with properties described in Chapter 2.

We also continue to assume that the precoder is sufficiently long so that we can model its output $y[n]$ effectively as a Gaussian random sequence. As Figure 4-1 indicates, the first stage of the decoding structure comprises three subsystems:

I: Linear Equalizer $b_1[n]$: Since the received signal $y[n]$ is effectively a Gaussian random sequence, the optimal estimator of the received sequence is a linear least square error (LLSE) estimator. In this system such an equalizer is identical to the optimum equalizer maximizing the SNR at the receiver [2].

II: FIR Filter $h[-n]$: This subsystem is aimed at recovering $x[n]$.

III: Symbol-by-Symbol Threshold Detector: Hardlimiter, *i.e.*, minimum distance receiver.

Tracking the signals through the channel, we have:

$$y_r[n] = a[n]y[n] + w[n] \,, \tag{4.1}$$

where $y_r[n]$ is the received signal. We will discuss the optimal equalizer later. Referring to Figure 4-1, we define the kernel $c_1[n]$ as

$$c_1[n] = a[n]b_1[n] \tag{4.2}$$

and $y_{r1}[n]$ as

$$y_{r1}[n] = c_1[n]y[n] + b_1[n]w[n] \,. \tag{4.3}$$

Furthermore, the postcoder output $x_{r1}[n]$ is

$$\begin{aligned} x_{r1}[n] &= h[-n] * y_{r1}[n] \\ &= h[-n] * (c_1[n] \cdot (x[n] * h[n])) + h[-n] * (w[n]b_1[n]) \end{aligned} \tag{4.4}$$

$$= f_1[n]x[n] + z_1[n] + u_1[n] ,$$

where the coefficient of $x[n]$ in this equation can be denoted as $f_1[n]$ with the following expression:

$$f_1[n] = c_1[n] * |h[-n]|^2 . \tag{4.5}$$

Moreover $z_1[n]$, the ISI caused by channel fading, can be written as

$$z_1[n] = \sum_{m \neq n} t_1[m]x[m] , \tag{4.6}$$

where $t_1[n]$ is a function of $a[n]$, $b_1[n]$ and $h[n]$, and the last term in (4.4) is the result of the channel additive noise

$$u_1[n] = h[-n] * (w[n]b_1[n]) . \tag{4.7}$$

To continue the process of using x_{r1} for further error reduction, we now take a closer look at each of the three components, introduced in equations above.

The weighting sequence $f_1[n]$: Assuming the precoder is sufficiently long, $f_1[n]$ for each n, as defined in (4.5), has an asymptotically Gaussian distribution. We wish to calculate the mean and variance of such a sequence. Since the precoder has unit energy, the mean of $f_1[n]$ is

$$\mu_{f1} = E(f_1[n]) = E(c_1[n] * |h[-n]|^2) = E(c_1[n]) = \mu_{c1} . \tag{4.8}$$

As for the variance of $f_1[n]$, we have

$$\text{var}(f1) = \text{var}(c_1[n] * |h[-n]|^2) = \sigma_{c1}^2 \sum_n h^4[n] = \frac{\sigma_{c1}^2}{\mathcal{D}_h} , \tag{4.9}$$

where the dispersion factor $\mathcal{D}_h$ is as defined in (2.12). Hence, $\text{var}(f_1[n]) \to 0$ as $\mathcal{D}_h \to \infty$, so we can effectively replace $f_1[n]$ with its mean, μ_{f1}. Using this

result (4.4) can be rewritten as:

$$x_{r1}[n] = \mu_{c1} x[n] + z_1[n] + u_1[n] \; . \tag{4.10}$$

The channel noise effect $u_1[n]$: This sequence, *cf.* (4.7), is an additive zero-mean Gaussian noise with variance

$$\text{var}(u_1[n]) = N \cdot E\left[|b_1[n]|^2\right] . \tag{4.11}$$

The ISI $z_1[n]$: Having a sufficiently long precoder also allows us to consider the ISI effectively a zero-mean Gaussian noise (*cf.* (4.6)).

In order to find the variance of $z_1[n]$ we consider the input and output of the FIR filter $h[-n]$ at the receiver. The fact that $h[n]$ is ideally an all-pass filter, *i.e.*, $|H(j\omega)| = 1$, implies that the energies of the two signals, $y_{r1}[n]$ and $x_{r1}[n]$, are equal. Using (4.3) and (4.10), we have:

$$\begin{aligned} \text{var}\left(y_{r1}[n]\right) &= \text{var}\left(x_{r1}[n]\right) \\ \sigma_{c1}^2 + \sigma_b^2 \sigma_w^2 &= \mu_{c1}^2 + \sigma_{z1}^2 + \sigma_b^2 \sigma_w^2 \; . \end{aligned} \tag{4.12}$$

As a result we find

$$\text{var}(z_1[n]) = \sigma_{c1}^2 \; . \tag{4.13}$$

Therefore, the postcoder output x_{r1}, is asymptotically a weighted version of the original symbol sequence $x[n]$, plus an effectively Gaussian noise. The latter itself is the sum of two uncorrelated Gaussian random sequences

$$v_1[n] = z_1[n] + w_1[n] \; . \tag{4.14}$$

It should also be mentioned that these results are identical to what we outlined in Chapter 2 (*cf.* (2.18)) [2].

We close this section by obtaining an expression for the optimal equalizer, $b_1[n]$.

The LLSE estimator for $y[n]$, based on observation of $y_r[n]$, is given by

$$b_1[n] = \frac{\langle y[n], y_r^*[n] \rangle}{\langle y_r[n], y_r^*[n] \rangle} = \frac{a^*[n]}{\langle a[n]y[n] + w[n], (a[n]y[n] + w[n])^* \rangle} = \frac{a^*[n]}{|a[n]|^2 + N} , \quad (4.15)$$

where the inner product is defined as

$$\langle u, v \rangle = E(uv) - E(u)E(v) \ . \quad (4.16)$$

4.2.2 Probability of Error Using the First Stage of the Postcoder

In this section we find the probability of error, as we will need it in the sequel for a comparative analysis of performance at each stage of the system. Considering (4.10), we note that the SNR at the output of filter $h[-n]$ in the receiver is

$$\gamma_1 = \frac{\mu_{c1}^2}{\sigma_{c1}^2 + N \cdot E[|b_1|^2]} \ . \quad (4.17)$$

Since we have modeled the system asymptotically as an additive Gaussian one, considering this SNR at the receiver we may write the probability of error in terms of the $Q(\cdot)$ function. In general, if an M-PSK sequence is to be transmitted through an AWGN channel, the probability of error per bit is given by

$$\Pr(\varepsilon) = Q\left(\frac{d_{\min}}{2}\sqrt{\beta}\right), \quad (4.18)$$

where $d_{\min}$ is the minimum Euclidean distance corresponding to the M-PSK sequence; and β is the ratio of the average energy of the M-PSK sequence to the variance of the complex noise *projected* onto the line connecting two adjacent symbols in the signal space. For example, for a binary sequence $M = 2$ with $d_{\min} = 2$ we have

$$\Pr(\varepsilon) = Q\left(\sqrt{\beta}\right) \ . \quad (4.19)$$

It is worth mentioning that β indeed can be written as a function of the SNR at the output of the transmitter. Using (2.28) we have shown that the SNR at the receiver can be written as

$$\gamma_1 = \frac{1}{\xi_0 e^{\xi_0} E_1(\xi_0)} - 1 \ , \tag{4.20}$$

where $\xi_0 = N$ is the inverse of the SNR of the output of the transmitter. We can also express the probability of error as a function of ξ_0. For $M > 2$, the independent additive noise and the ISI effects are both *complex* Gaussian, thereby making the value of β twice that of the SNR calculated at the receiver. At this stage of the precoder, then, we have

$$\Pr(\varepsilon) = Q\left(d_{\min}\sqrt{\frac{\gamma_1}{2}}\right) \ . \tag{4.21}$$

However, for the binary sequence $M = 2$, there is a slight difference. Although the ISI effect is still Gaussian in the limiting case, this component is purely *real*, in contrast to the case $M > 2$. Therefore, in the binary case the variance of the noise projected onto the line connecting the two symbols ± 1, is

$$\sigma_{c1}^2 + \frac{N \cdot E[|b_1|^2]}{2} \ .$$

Hence, β_1 as a function of the calculated SNR, γ_1 is given by

$$\beta_1 = \frac{1}{\frac{1}{\gamma_1} + \frac{N \cdot E[|b_1|^2]}{2\mu_{c1}^2}} \ . \tag{4.22}$$

Furthermore, both μ_{c1} and $E[|b_1|^2]$ can be calculated as a function of ξ_0, These results are developed in *cf.* Appendix A. Recall that in Chapter 2 we obtained results using the first stage with a 4-PSK sequence; see Figure 2-5 which also depicts the AWGN performance. The probability of error nonlinearly diverges as the SNR is increased and this increasing difference corresponds to the ISI effects which come into play especially at high SNRs. Having acquired a reasonable estimate $\hat{x}_1[n]$ of the original symbol sequence $x[n]$, as well as a good model for the channel fading parameters, we now continue our effort to eliminate the ISI effects in the subsequent decoding stages.

4.2.3 Second Stage of the Postcoder

At the output of the first stage we have $\hat{x}_1[n]$ as the estimate for $x[n]$. Using this estimated sequence we want to estimate the ISI of the received signal and reduce the error caused by this factor. One alternative is to use this estimated sequence $\hat{x}_1[n]$ and pass it through a simulated channel model. By so doing we can use the generated ISI as an estimate for the original ISI. In order to use such a procedure, first we must calculate the correlation of the estimated sequence with $x[n]$. We will subsequently show that this parameter is relevant to combatting the ISI.

For $\hat{x}_1[n]$ the output of the hardlimiter, we have (*cf.* Figure 4-1)

$$\hat{x}_1[n] = x[n] + e_1[n], \tag{4.23}$$

where the conditional probability mass function for $e_1[n]$ given $x[n]$, can be written as:

$$\Pr(e_1[n] \mid x[n]) = \begin{cases} 1 - Q(\sqrt{\beta_1}) & e_1[n] = 0 \\ Q(\sqrt{\beta_1}) & e_1[\mathrm{n}]{=}{-}2x[n] \\ 0 & \text{otherwise} \end{cases} . \tag{4.24}$$

Since $x[n]$ and $\hat{x}_1[n]$ are binary-valued and have unit variance, we note that

$$\begin{aligned} E(x \cdot e_1) &= \Pr(x = 1)E(x \cdot e_1 | x = 1) + \Pr(x = -1)E(x \cdot e_1 | x = -1) \\ &= -2Q(\sqrt{\beta_1}) . \end{aligned} \tag{4.25}$$

We now introduce a variable which will play a central role in the remainder of our discussion: the correlation of $x[n]$ with $\hat{x}_1[n]$ which is given by

$$\rho_1 = E(x \cdot \hat{x}_1) = E(x \cdot (x + e_1)) = E(x^2) + E(x \cdot e_1) = 1 - 2Q(\sqrt{\beta_1}) . \tag{4.26}$$

New equalizer

Recall that the purpose of using the equalizer in the first stage was to use the received sequence, and estimate the output of the transmitter by knowing the additive

noise model and the exact fading coefficient. At this point we also wish to exploit information contained by the estimated signal from the first stage. Therefore, the new equalizer is given by

$$b_2[n] = \frac{\langle y[n], y_r^*[n]\rangle|\hat{x}_1}{\langle y_r[n], y_r^*[n]\rangle|\hat{x}_1} = \frac{a^*[n]\text{var}(y[n]\ |\hat{x}_1)}{|a[n]|^2\text{var}(y[n]|\hat{x}_1) + \text{var}(w[n]|\hat{x}_1)}\ , \tag{4.27}$$

Considering a sufficiently large losslessness factor $\mathcal{L}_h$ for the precoder, *i.e.* $h[n] * h[-n] \approx \delta[n]$, it can be shown that

$$\text{var}(y|\hat{x}_1) = \text{var}(x|\hat{x}_1). \tag{4.28}$$

In order to find the right hand side of this equation we use the computed correlation factor ρ_1 (*cf.* (4.26))

$$\text{var}(x|\hat{x}_1) = 1 - \rho_1^2. \tag{4.29}$$

Therefore the equalizer at this stage is

$$\begin{aligned} b_2[n] &= \frac{a^*[n]\text{var}(x[n]|\hat{x}_1)}{|a[n]|^2\text{var}(x[n]|\hat{x}_1) + \text{var}(w[n])} \\ &= \frac{a^*[n](1-\rho_1^2)}{|a[n]|^2(1-\rho_1^2) + N}. \end{aligned} \tag{4.30}$$

With this new equalizer the product of the fading coefficient and the equalizer is given by

$$c_2[n] = a[n]b_2[n] = \frac{|a[n]|^2}{|a[n]|^2 + \frac{N}{1-\rho_1^2}}. \tag{4.31}$$

Therefore, the output of the equalizer at this stage of system, Figure 4-2, is given by

$$y_{r2}[n] = c_2[n]y[n] + b_2[n]w[n]\ , \tag{4.32}$$

and the output of the FIR filter $h[-n]$, shown in Figure 4-2, is similar to what we had for the first stage of the postcoder

$$x_{r2}[n] = h[-n] * (c_2[n] \cdot (x[n] * h[n])) + h[-n] * (w[n]b_1[n]) \tag{4.33}$$

$$= f_2[n]x[n] + z_2[n] + u_2[n] \, .$$

Similar to what we had for the first stage the relevant parameters are as follows.

- $f_2[n]$ is the weighting sequence $f_2[n] = c_2[n] * |h[-n]|^2$.
- $z_2[n]$ is the ISI component $z_2[n] = \sum_{m \neq n} t_2[m]x[m]$ where $t_2[n]$ is a function of $a[n]$, $b_2[n]$ and $h[n]$.
- $u_2[n]$ is the noise caused by the channel additive noise, $u_1[n] = h[-n] * (w[n]b_1[n])$.

To find the second-order statistics of these sequences we may use the same method described for the first stage of the postcoder. For example, we note that the zero-mean ISI component of x_{r2} is an asymptotically Gaussion additive noise. Exploiting the fact that the two sequences $t_2[n]$ and $x[n]$ are independent, we write the ISI variance as follows:

$$\begin{aligned} \text{var}(z_2) &= \sum_{m \neq n} \text{var}(t_2[m]x[m]) = \sum_{m \neq n} E(|t_2[m]|^2) \cdot E(|x[m]|^2) \\ &= \sum_{m \neq n} E(|t_2[m]|^2) \, . \end{aligned} \tag{4.34}$$

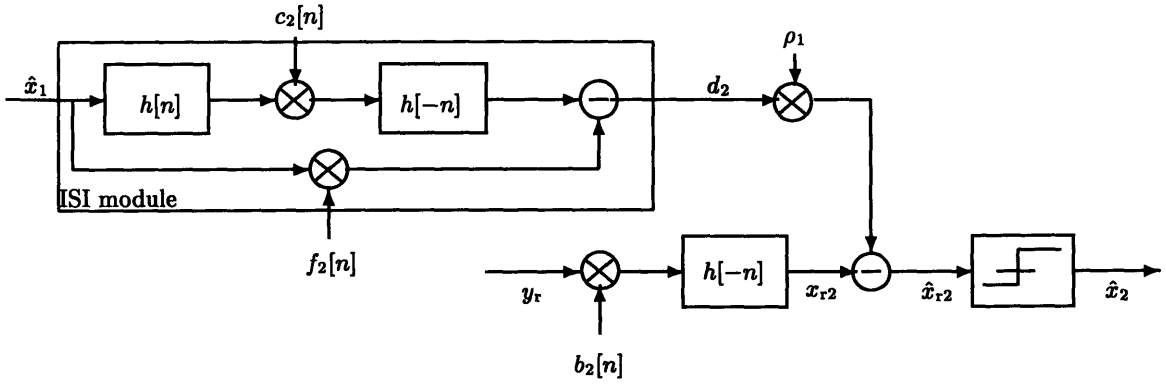

Figure 4-2: Second stage of the postcoder

ISI Module

At this point we regenerate the estimated ISI. This part of the postcoder appears boxed in Figure 4-2. By passing the estimated signal through the simulated channel,

which does not have any additive noise, the only unwanted component that would be generated is the estimated ISI, $d_2[n]$:

$$d_2[n] = \sum_{m \neq n} t_2[m]\hat{x}_1[m]. \tag{4.35}$$

This estimated component will then be used for the ISI reduction which we describe in following section.

ISI Reduction and Signal Detection

Considering the original ISI variance, (4.35), we can calculate the variance of the ISI component of x_{r2}, given the detected sequence from the first stage $\hat{x}_1$:

$$\begin{aligned} \mathrm{var}(z_2|\hat{x}_1) &= \sum_{m \neq n} \mathrm{var}(t_2[m]|\hat{x}_1) \cdot \mathrm{var}(x[m]|\hat{x}_1) \\ &= \mathrm{var}(x|\hat{x}_1) \sum_{m \neq n} \mathrm{var}(|t_2[m]|^2|) \\ &= (1-\rho_1^2)\sigma_{c2}^2 \,. \end{aligned} \tag{4.36}$$

This variance, which is less than that of the original ISI, shows the maximum possible reduction in ISI variance using $\hat{x}_1[n]$. As Figure 4-2 indicates, by constructing $\hat{x}_{r2}[n] = x_r[n] - \rho_1 d_2[n]$, we can achieve maximum possible improvement. The new sequence $\hat{x}_{r2}[n]$ has the ISI component

$$\hat{z}_2[n] = z_2[n] - \rho_1 d_2[n] \,. \tag{4.37}$$

It can be shown that the variance of this new ISI is equal to $\mathrm{var}(z_2|\hat{x}_1)$ calculated in (4.36)

$$\mathrm{var}(\hat{z}_2[n]) = (1-\rho_1^2)\sigma_{c2}^2 \,. \tag{4.38}$$

Last, we have the estimated sequence at the second stage as

$$\hat{x}_2[n] = f_2[n]x[n] + \hat{z}_2[n] + u_2[n] \,. \tag{4.39}$$

In the following section we find the probability of error with this new estimated sequence.

4.2.4 Probability of error at the Second Stage of the Postcoder

Using the same method we used for the first stage, to find the SNR at the input of the hardlimiter in the second stage we have (*cf.* Figure 4-2)

$$\gamma_2 = \frac{\mu_{c2}^2}{(1-\rho_1^2)\sigma_{c2}^2 + N \cdot E[|b_2|^2]} \,. \tag{4.40}$$

Furthermore, as we calculated in Appendix B, this SNR can be written as a function of the SNR at the output of the transmitter, and the correlation factor ρ_1

$$\gamma_2 = \frac{1}{(1-\rho_1^2)}\left(\frac{1}{\xi_1 e^{\xi_1} E_1(\xi_1)} - 1\right) , \tag{4.41}$$

where

$$\xi_1 = \frac{N}{(1-\rho_1^2)}. \tag{4.42}$$

The probability of error, which has the same expression as that of the first stage, can be written as a function of β_2

$$\Pr(\varepsilon) = Q\left(\sqrt{\beta_2}\right) , \tag{4.43}$$

where β_2 can be obtained by performing calculations similar to those of the first stage,(*cf.* (4.22))

$$\beta_2 = \frac{1}{\frac{1}{\gamma_2} + \frac{N \cdot E[|b_2|^2]}{2\mu_{c2}^2}} \,, \tag{4.44}$$

where μ_{c1} and $E[|b_1|^2]$ can be calculated as function of ξ_1 (see Appendix A). We can use the same strategy and add more stages to the postcoder. In general, β_i can be

written as a function of ξ_i, which at stage i is defined as

$$\xi_i = \frac{N}{(1-\rho_i^2)}, \tag{4.45}$$

and in general at each stage we have, based on (4.44),

$$\beta_{i+1} = S(\xi_i), \tag{4.46}$$

where for a particular transmitted SNR, fixed N, $S(\cdot)$ is a monotonically increasing function. Since at each stage the correlation increases, ξ_i also increases, thereby causing an increase in β_i. Consequently, the probability of error would decrease at each stage. Although each stage improves the performance, there is a limit to which probability of error can be decreased. Namely, for each transmitted SNR there is a certain number of useful stages which could noticeably improve the performance. Section 4.2.6 will discuss this process in more detail.

4.2.5 Simplifying the Computation

Adding each stage to the postcoder increases the computational complexity and decoding delay, while improving the probability of error performance. However, we can keep the mentioned computational problem and unwanted delay under control by using an LPTV system as the precoder. Since individual $h_i[n]$'s in the LPTV precoder are $\pm h$, all multiplications are converted to summations. For example, for the weighting secuence $f_i[n]$, we have

$$f_i[n] = c_i[n] * |h[-n]|^2 = h^2 \sum c_i[n] \, . \tag{4.47}$$

In addition, since the variance of $f_i[n]$ is small, we may replace it by its mean without affecting the behavior of the system at each stage. Referring to Appendix A, note that

$$\mu_{fi} = \mu_{ci} = 1 - \xi_i e^{\xi_i} E_1(\xi_i) \, , \tag{4.48}$$

where ξ_i is as in (4.45).

4.2.6 Probability of Error Using the Multistage Postcoder

In the multistage postcoder discussed above, the successive iterations in computing the probability of error may be represented in state-space form. As we discussed previously, at each stage the probability of error can be written as a function of ξ_i. Using (4.46), the probability of error at each stage can be written as

$$Q(\sqrt{\beta_{i+1}}) = Q(\sqrt{S(\xi_i)}) \,. \tag{4.49}$$

By substituting ξ as a function of ρ, *cf.* (4.45), we can rewrite the probability of error as some function of ρ_i

$$Q(\sqrt{\beta_{i+1}}) = G(\rho_i) \,. \tag{4.50}$$

On the other hand, in order to calculate ρ for the next stage we use (4.26), which can be rewritten as

$$Q(\sqrt{\beta_{i+1}}) = \frac{1-\rho_{i+1}}{2} \,. \tag{4.51}$$

Therefore, the state-space time evolution equation is of the form:

$$G(\rho_i) = \frac{1-\rho_{i+1}}{2} \,. \tag{4.52}$$

Although ρ_i appeared in the equations beginning with the second stage, the equations corresponding to the first stage can clearly be thought of as a special case wherein $\rho = 0$. Figure 4-3 shows the two functions, $G(\cdot)$ and $Q(\cdot)$, for different SNRs. In the first stage, the probability of error corresponds to $\rho = 0$. In order to find the probability of error corresponding to the second stage, we draw a horizontal line at height $Q(0)$. Let the point of intersection of this line with $G(\cdot)$ be located at $\rho = \rho_2$. Then the probability of error corresponding to the second stage is simply $Q(\rho_2)$.

Therefore, $Q(0)$, shown in the left side of Figure (4-3), corresponds to the probability of error of the first stage. As $\rho \longrightarrow 1$, Figure (4-3) shows that $\Pr(\varepsilon)$ approaches

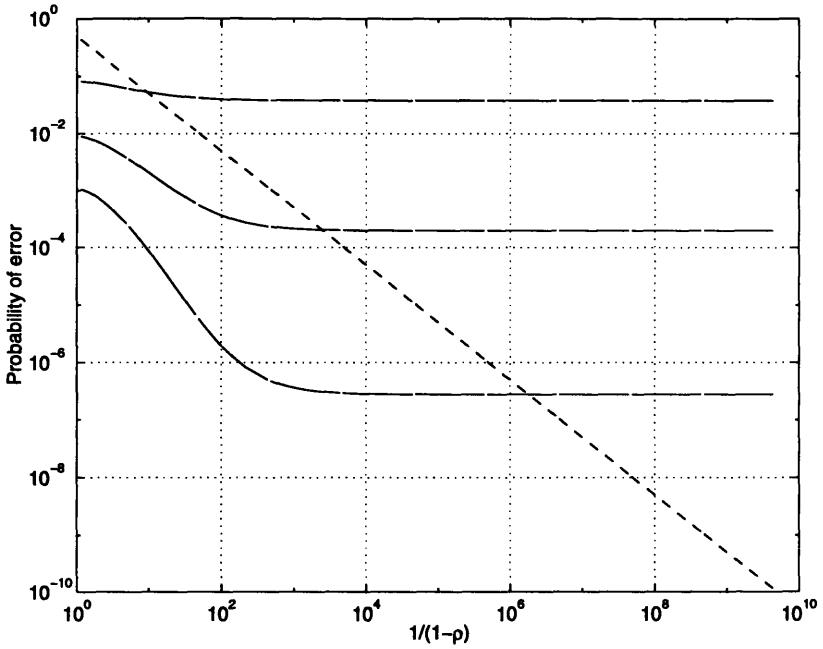

Figure 4-3: *Dashed line is $G(\rho)$ and the successively lower solid curves represent $Q(\rho)$ for SNR = 2,8,11, respectively, assuming the binary sequence as the transmitted sequence.*

that of the AWGN channel, *i.e.*, (4.40) with $\rho = 1$.

However, it is clear that the intersection of the two curves $Q(\cdot)$ and $G(\cdot)$ marks the limiting probability of error which we can obtain using the Newton iteration method in this state-space model. Therefore, the achievable performance with this method is the solution to following equation:

$$G(\rho) = \frac{1-\rho}{2} . \tag{4.53}$$

Figure 4-3 clearly shows that for low SNRs we can never reach the AWGN channel performance, while as the SNR increases, the intersection mentioned earlier approaches the AWGN probability of error. Moreover, the figure also indicates that for SNRs higher than 12dB only one stage, in addition to the first, is needed to significantly improve the performance.

4.2.7 Performance

All the experiments in this section have been carried out using an LPTV precoder with a length of 256. Results of using this method for 8dB are depicted in Table 4.1 .

$i=$	1	2	3	4	5	6	7
ρ_i	0.9641	0.9966	0.9990	0.9992	0.9992	0.9992	0.9992
$\Pr(\varepsilon)$	0.0180	0.0017	0.0005	4.23×10^{-4}	4.18×10^{-4}	4.17×10^{-4}	4.17×10^{-4}
μ_c	0.7368	0.2582	0.0392	0.0122	0.0104	0.0103	0.0103

Table 4.1: Performance of cascaded stages for SNR=8dB.

For AWGN channel in this case: $\Pr(\varepsilon) = Q\sqrt{2/N} = 1.9091 \times 10^{-4}$.

As the table shows, in the first and second stages there is significant performance improvement, while beginning with the third stage the improvement slows down. Table 4.2 shows the result for an SNR of 11dB. In this case after four stages the probability of error flattens. This indicates that there is no need to have more stages. Note also that for this case the probability of error after four stages is close to that of the AWGN channel performance. The probability of error achievable by this method

$i=$	1	2	3	4	AWGN
ρ_i	0.9957	0.9999...	0.9999...	0.9999...	
$\Pr(\varepsilon)$	0.0021	1.5406×10^{-6}	5.5168×10^{-7}	5.5136×10^{-7}	5.2261×10^{-7}
μ_c	0.8251	0.0893	7.7251×10^{-5}	2.7666×10^{-5}	

Table 4.2: Performance of cascaded stages for SNR=11dB.

is shown in Figure 4-4. As we can see the performance is almost identical to that of AWGN channel for high SNRs.

We have used MATLAB for simulating this algorithm. As the SNR increases it is likelier for early stages to have ρ_i very close to one. Therefore MATLAB fails to calculate the real $\xi_i e^{\xi_i} E_1(\xi_i)$. For such cases the following approximation is used [11]

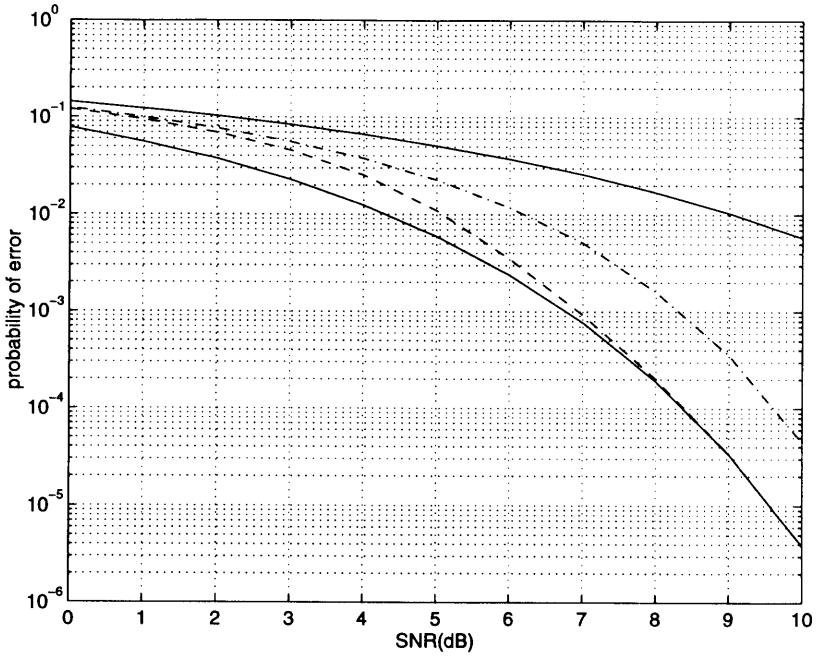

Figure 4-4: *Probability of error for binary sequence in fading channel: The successively lower solid curves denote the performance of the first stage of postcoder and the AWGN channel performance, respectively. The dash-dotted curve is the performance achievable by using enough postcoder stages at the receiver.*

$(\xi_i = N/(1-\rho_i^2) \gg 1)$:

$$\xi_i e^{\xi_i} E_1(\xi_i) = \frac{\xi_i^2 + 2.334733\xi_i + .250621}{\xi_i^2 + 3.330657\xi_i + 1.681534}. \tag{4.54}$$

4.3 Frequency-Selective Fading Channel

We can use the same multistage scheme for the frequency-selective case. The first stage is the same as what we introduced in Chapter 2, while the second stage is shown in Figure 4-5. In this model the equalizer frequency response is

$$B_i(\omega; n] = \frac{A^*(\omega; n]}{|A(\omega; n]|^2 + \frac{N}{1-\rho_i^2}} \tag{4.55}$$

and $C_i(\omega; n]$, as defined in Chapter 2, is

$$C_i(\omega; n] = A(\omega; n] B_i(\omega; n] \; . \tag{4.56}$$

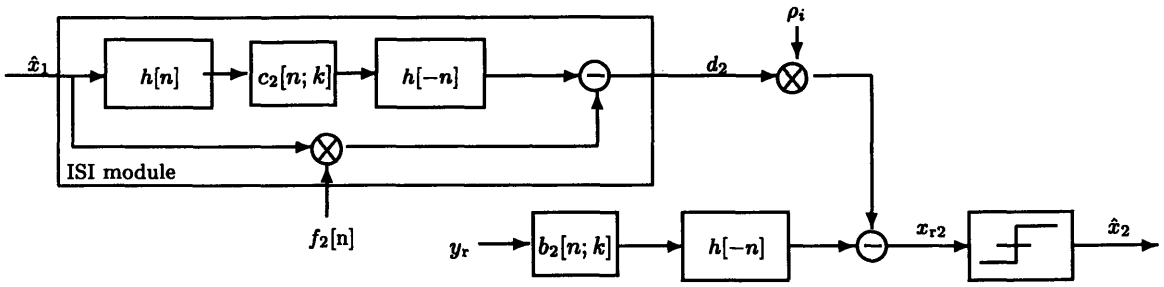

Figure 4-5: Second stage of the postcoder in frequency-selective channel

Furthermore, the weighting sequence $f_i[n]$ can be defined as:

$$f_i[n] = \sum_k H_k[n] * c[n;k] \,. \tag{4.57}$$

Each $H_k[n]$ in the equation above can be calculated as we track the coefficient of $x[n]$ in the expression for $x_r[n]$, obtained in the following matrix form of the system model:

$$\begin{bmatrix} \vdots \\ x_r[n+1-l] \\ x_r[n+2-l] \\ x_r[n+3-l] \\ \vdots \end{bmatrix} = \underbrace{\begin{bmatrix} \vdots & \vdots & \cdots \\ h[l+1-n] & h[l+2-n] & \cdots \\ h[l-n] & h[l+1-n] & \cdots \\ h[l-1-n] & h[l-n] & \cdots \\ \vdots & \vdots & \ddots \end{bmatrix}}_{\text{postcoder}} \times$$

$$\begin{bmatrix} \vdots & \vdots & \cdot \\ c[n;n-1] & c[n;n-2] & \cdot \\ c[n+1;n] & \cdot & \cdot \\ \vdots & c[n+2;n] & \cdot \\ \vdots & \vdots & \cdot \end{bmatrix} \underbrace{\begin{bmatrix} \vdots & \vdots & \cdot \\ h[n] & h[n-1] & \cdot \\ h[n+1] & h[n] & \cdot \\ h[n+2] & h[n+1] & \cdot \\ \vdots & \vdots & \cdot \end{bmatrix}}_{\text{precoder}} \begin{bmatrix} \vdots \\ x[n] \\ x[n+1] \\ x[n+2] \\ \vdots \end{bmatrix} .$$

Note that $H_0[n]$ is the coefficient of $x[n]$, $f[n]$, in the frequency-nonselective case. The correlation factor ρ_i has the same definition as (4.26). In this case, the probability of

error at each stage is the same as in (4.19) and γ is defined as

$$\gamma_{i+1} = \frac{1}{(1-\rho_i^2)}\left(\frac{1}{\xi_i e^{\xi_i} E_1(\xi_i)} - 1\right), \tag{4.58}$$

where ξ is defined in (4.45).

4.4 M-PSK Sequences in Fading Channel with Precoder and Multistage Postcoder

It is also worth mentioning that we can generalize our binary PSK results to M-PSK sequences. The procedure is the same as that in the binary case, except that the probability density for e_1, *cf.* (4.24), is different, as is the expression for ρ in (4.26).

For example, when we use a 4-PSK sequence for sending the data over the fading channel, four symbols, $1, -1, j$, and $-j$ in the complex plane are considered. The probability of error at each stage is given by (4.21), with $d_{min} = \sqrt{2}$

$$\Pr(\varepsilon) = Q(\sqrt{\gamma_i}), \tag{4.59}$$

where γ_i is the same as in (4.17). The probability density of $e_i[n]$ at each stage, given $x[n] = 1$, is:

$$\Pr(e_i[n]|x[n]=1) = \begin{cases} 1 - Q(\sqrt{\gamma_i}) & e_i[n] = 0 \\ Q(\sqrt{2\gamma_i})/2 & e_i[n] = 1 + j \\ Q(\sqrt{2\gamma_i})/2 & e_i[n] = 1 - j \\ 0 & \text{otherwise} \end{cases}, \tag{4.60}$$

and similar expressions for this density hold, when $x[n]$ takes on one of the other three symbol values, -1, j, and $-j$. In this case we have

$$E(x \cdot e_i) = \sum Pr(s) E(x \cdot e_i | x = s) = -Q(\sqrt{\gamma_i}), \tag{4.61}$$

where s represents the four possible symbols.

Repeating the procedure yields the achievable probability of error given by

$$Q(\sqrt{\gamma}) = 1 - \rho, \tag{4.62}$$

where ρ satisfies the following equation:

$$G(\sqrt{\rho}) = 1 - \rho, \tag{4.63}$$

and $G(\cdot)$ is the expression for probability of error as a function of ρ. Results of the performance in this case are shown in Figure (4-6).

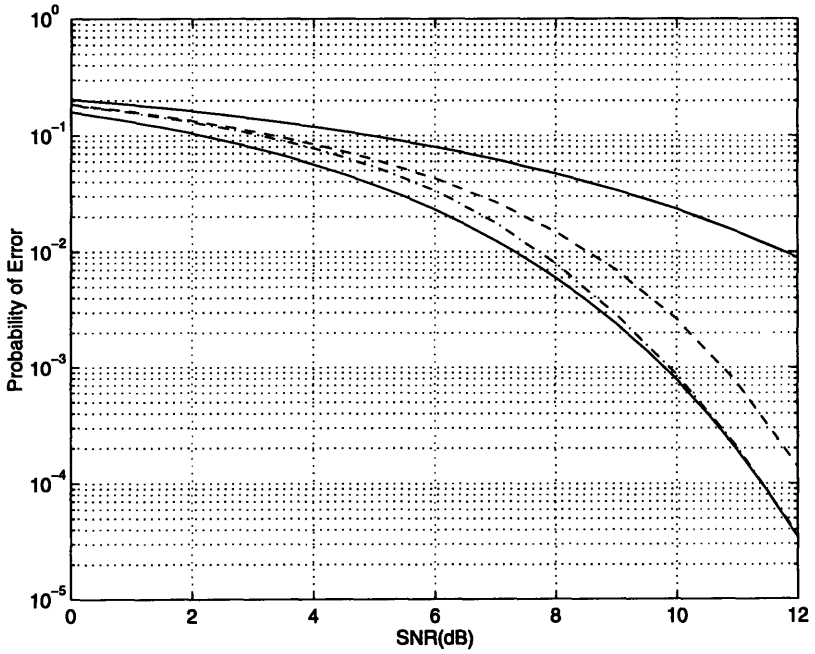

Figure 4-6: *Probability of error for 4-PSK sequence: The successively lower solid curves correspond to the performance of the first stage of the postcoder in a fading channel, and the AWGN channel performance, respectively. The dashed curve is the performance adding one more stage to the postcoder. The dash-dotted curve is the performance achievable by using enough postcoder stages at the receiver.*

Chapter 5

Conclusion

The goal of this research has been to improve the probability of error performance in fading channels using spread-response precoding. We have used two different approaches to the problem. Adding the trellis coded modulation (TCM) has been shown to improve the performance. However, delay in decoding, as well as the cost and complexity of such a system is also of concern to us. Also the improvement due to the proposed scheme is not considerable at low SNRs.

Nevertheless, the design of trellis coders to achieve optimum performance on the fading channel is guided by a more complicated factor than in the AWGN channel. The fact that by using spread-response precoder in a fading channel we are working with an effectively AWGN model makes the problem identical to the design of a trellis coder for an AWGN channel; the latter, is a well-developed and experimented problem.

Another avenue of attack on the problem is the use of a multistage postcoder in the receiver which, as has been shown, has led to significant improvement in the probability of error performance. Using the first method, the trellis coder is implemented to remove the additive noise of the signal. However, the major problem to be dealt with, especially at high SNRs, is the intersymbol interference, something which the TCM fails to address. On the other hand, the multistage postcoder exclusively attempts to remove the ISI while not addressing the additive white Gaussian noise. Consequently, the multistage postcoder, in substantially combatting the ISI, converts

the performance to that of an AWGN channel model, especially at high SNRs.

In the multistage scheme computational complexity and time delay issues arise. The maximum time delay at each stage is on the order of the length of the precoder, and it may indeed be comparable that of trellis decoding. However, as discussed in Chapter 4, for high SNRs, adding one stage to the usual postcoder is sufficient to yield considerably higher performance.

In order to have a better performance than that yielded by these two methods in high SNRs, we can also use a combination of TCM and multistage postcoder in the receiver. In this situation the tradeoff between time delay in the decision process and the quality of performance should be considered. This hybrid method may prove to be an interesting direction of future research.

As another direction, note that in the work of this thesis we have assumed a perfect knowledge of the fading coefficient in the receiver. The sensitivity of the system performance to this parameter is an important topic of future research. Specifically, in multistage postcoding the key parametars are very sensitive to both the SNR of the transmitted sequence and the fading coefficient. Robustness methods for desensitizing the algorithm to such elements is another further challenge that can be addressed in future work.

Furthermore, the theoretical results of the frequency-selective channel which we have developed should be paired against simulated results, and performances should be compared.

It is also worth mentioning that the multistage postcoder scheme may be useful in applications involving multiuser channels and this represents a promising direction for future work.

Appendix A

Computation of μ_C and $E(|b|^2)$

Considering $a[n]$, coefficient of fading in a frequency-nonselective fading channel, we have:

$$a[n] = a_{\mathrm{r}}[n] + a_{\mathrm{i}}[n] \ , \tag{A.1}$$

where each of the components real and imaginary part of $a[n]$, are independent identically distributed (i.i.d) Gaussian r.v.'s,

$$Var(a_{\mathrm{r}}) = Var(a_{\mathrm{i}}) = \frac{\sigma_a^2}{2} \ , \tag{A.2}$$

where σ_a^2 is variance of $a[n]$. Therefore the probability density of $a[n]$ far all n is:

$$P_a(z) = P_{a_{\mathrm{r}}}(x) P_{a_{\mathrm{i}}}(y) = \frac{1}{\pi\sigma_a^2} e^{-\frac{(x^2+y^2)}{2}} \ , \tag{A.3}$$

and the absolute value of a has a Rayleigh distribution:

$$P_{|a|}(s) = \frac{2s}{\sigma_a^2} e^{-\frac{s^2}{\sigma_a^2}} \ . \tag{A.4}$$

First we calculate the expected value of $c[n]$:

$$E(c[n]) = E\left(\frac{|a|^2}{|a|^2+\xi}\right) = \int_0^\infty \frac{s^2}{s^2+\xi}\left(\frac{2\rho}{\sigma_a^2} e^{-\frac{s^2}{\sigma_a^2}}\right) ds \ . \tag{A.5}$$

Changing variable s^2 to u and u to $t-\xi$ yields

$$E(c[n]) = \int_0^\infty \frac{u}{u+\xi}\left(\frac{1}{\sigma_a^2}e^{-\frac{u}{\sigma_a^2}}\right)du = \int_\xi^\infty \frac{t-\xi}{t\sigma_a^2}e^{-\frac{(t-\xi)}{\sigma_a^2}}du \ , \tag{A.6}$$

Therefore we have:

$$\mu_c = E(c[n]) = 1 - \frac{\xi}{\sigma_a^2}e^{\frac{\xi}{\sigma_a^2}}\int_\xi^\infty \frac{e^{-t}}{t}dt = 1 - \frac{\xi}{\sigma_a^2}e^{\frac{\xi}{\sigma_a^2}}E_1(\xi) \ . \tag{A.7}$$

Computation of $E(|b|^2)$:

$$E(|b|^2) = E\left(\frac{|a|^2}{(|a|^2+\xi)^2}\right) = \int_0^\infty \frac{s^2}{(s^2+\xi)^2}\left(\frac{2s}{\sigma_a^2}e^{-\frac{s^2}{\sigma_a^2}}\right)ds \ . \tag{A.8}$$

Using the same change of variable we used for computing μ_c ($\sigma_a^2 = 1$) :

$$E(|b|^2) = \int_0^\infty \frac{u}{(u+\xi)^2}e^{-u}du = \int_\xi^\infty \frac{t-\xi}{t^2}e^{-(t-\xi)}du \ , \tag{A.9}$$

Therefore we have

$$E(|b|^2) = e^\xi E_1(\xi) + \xi e^\xi E_1(\xi) - 1, \tag{A.10}$$

as a function of ξ.

Appendix B

Computation of γ

In general at each stage for the SNR of the output of the postcoder we have:

$$\gamma_i = \frac{|E(ab_i)|^2}{(1-\rho_{i-1}^2)var(ab_i) + N(E(|b_i|^2))}. \tag{B.1}$$

Which can be written as:

$$\gamma_i = \frac{1}{\frac{1}{\phi(b_i)} - (1-\rho_{i-1}^2)}, \tag{B.2}$$

where

$$\phi(b_i) = \frac{|E(ab_i)|^2}{E[(1-\rho_{i-1}^2)|ab_i|^2 + N|b_i|^2]}. \tag{B.3}$$

Using Schwartz inequality:

$$\begin{aligned} |E(ab_i)|^2 &= \left| E\left[\frac{a}{\sqrt{(1-\rho_{i-1}^2)|a|^2 + N}} . b_i \sqrt{(1-\rho_{i-1}^2)|a|^2 + N} \right] \right|^2 \\ &\leq E\left[\frac{|a|^2}{(1-\rho_{i-1}^2)|a|^2 + N} \right] E\left[((1-\rho_{i-1}^2)|a|^2 + N)|b_i|^2 \right], \end{aligned} \tag{B.4}$$

with the equality for

$$b_i \propto \frac{a^*}{(1-\rho_{i-1}^2)|a|^2 + N}. \tag{B.5}$$

Using this equalizer, we can substitute $\phi(b_i)$ with:

$$\phi(b_i) = \frac{1}{1-\rho_{i-1}^2} E\left[\frac{|a|^2}{(|a|^2 + \frac{N}{1-\rho_{i-1}^2})}\right]. \tag{B.6}$$

Considering Equation(A.5):

$$\phi(b_i) = \frac{1}{1-\rho_{i-1}^2}\left(1 - \xi_{i-1} e^{\xi_{i-1}} E_1(\xi_{i-1})\right), \tag{B.7}$$

with $\xi_{i-1} = \frac{N}{1-\rho_{i-1}^2}$. If we substitute $\phi(b_i)$, Equaiton (B.7), in Equaiton (B.2), γ_i is

$$\gamma_i = \frac{1}{1-\rho_{i-1}^2}\left(\frac{1}{1 - \xi_{i-1} e^{\xi_{i-1}} E_1(\xi_{i-1})} - 1\right), \tag{B.8}$$

as a function of ρ_{i-1} and ξ_{i-1}.

Bibliography

[1] J. G. Proakis. *Digital Communications.* New York NJ:McGraw-Hill, second edition, 1989.

[2] Greg W. Wornell. "Spread-Response Precoding for Communication over Fading Channels". To appear in *IEEE Trans. Inform. Theory.*

[3] Greg W. Wornell. "Spread-Response CDMA: Efficient Multiuser Communication in the Presence of Fading ". To appear in *IEEE Trans. Inform. Theory.*

[4] P. McLane, M. Simon, E. Biglieri, D. Divsalar. *Introduction to Trellis-Coded Modulation with Applications.* New York NY:Mcmillan Publishing Company, 1991.

[5] Gottfried Ungerboeck. "Trellis-Coded Modulation with Redundant Signal Sets. Part I: Introduction". *IEEE Commun, Magazine*, 25(2), February 1987.

[6] Gottfried Ungerboeck. "Trellis-Coded Modulation with Redundant Signal Sets. Part II: State of art". *IEEE Commun. Magazine*, 25(2), 1987.

[7] Daryush Divsalar. "The Design of Trellis-Coded M-PSK for Fading Channels: Performance criteria". *IEEE Trans. Commun.*, 36(9), 1988.

[8] Ephrahaim Zehavi. "8-PSK Trellis Codes for a Rayleigh Channel". *IEEE Trans. Commun.*, 40(5), May 1992.

[9] G. David Forney. "Maximum-Likelihood Sequence Estimation of Digital Sequences in Precense of Intersymbol Interferene". *IEEE Trans. Inform. Theory.*

[10] A. Wittneben. "A Novel Bandwidth Efficient Analog Coding/Decoding Scheme for Data Transmission over Fading Channels Performance Criteria". *Proc. IEEE GLOBECOM*, 1994.

[11] M. Abramowitz and I. A. Stegun. *Handbook of Mathematical Functions.* New York: Dover, thenth edition, 1972.

5224-10